THE UNIVERSITY OF OKLAHOMA

GRADUATE COLLEGE

THE VISIBLE RADIATION FROM HELIUM IN A STRONG SHOCK WAVE

A DISSERTATION

SUBMITTED TO THE GRADUATE FACULTY

in partial fulfillment of the requirements for the

degree of

DOCTOR OF PHILOSOPHY

BY

GLENN E. SEAY

Norman, Oklahoma

1957

Downloaded from SHAREOK. Persistent Handle URL: https://hdl.handle.net/11244/246

THE VISIBLE RADIATION FROM HELIUM IN A STRONG SHOCK WAVE

APPROVED BY

R. D. Fowler

Wm Schrieve

Otto Theimer

Arthur Bernhart

J E La Fon

DISSERTATION COMMITTEE

ACKNOWLEDGMENTS

The author wishes to express his gratitude to Dr. L. B. Seely, Jr., for suggesting the problem and for his continued guidance and encouragement; to Professor R. G. Fowler for his stimulating suggestions and support; to Dr. Bennett Kivel for his theoretical contributions; and to J. O. Johnson for his invaluable technical criticism and assistance.

The author wishes to thank Dr. R. E. Duff for providing the hydrothermodynamic data from an IBM 704 Data Processing Machine; and Dr. Duff, Professor G. H. Dieke, Professor N. R. Davidson, Dr. R. E. Meyerott, Dr. W. W. Wood, and Dr. Wildon Fickett for many interesting and helpful discussions.

This research was performed as a part of the Graduate Thesis Program of the Los Alamos Scientific Laboratory in cooperation with the University of Oklahoma.

TABLE OF CONTENTS

		Page
LIST OF TABLES		v
LIST OF ILLUSTRATIONS		vi
Chapter		
I.	INTRODUCTION	1
II.	APPARATUS	6
	Explosive Shock Tube	6
	Smear Camera	9
	Smoke Shutter and Monitor	13
	Spectrograph	14
	Electrodeless Discharge	14
	Photographic Material	14
III.	EXPERIMENTAL ARRANGEMENTS AND PROCEDURES	17
	Time-integrated Spectra	18
	Time-resolved Spectra	22
	Spectrographic Plate Calibration	28
IV.	DATA AND ANALYSIS	30
	Qualitative Data	30
	Spectrograms	32
	Smear Camera Photographs	42
V.	HYDROTHERMODYNAMIC CALCULATIONS	47
VI.	COMPARISON WITH THEORY	69
	Line Broadening and Shift	69
	Self-absorption Broadening	83
	Depression of the Series Limits	85
	Forbidden Lines	87
	Continuum Radiation	91
VII.	SUMMARY, CRITIQUE, AND SUGGESTIONS FOR FUTURE EXPERIMENTS	95

LIST OF TABLES

Table		Page
I.	Data from Time-integrated Spectra.....	38
II.	Data from Time-resolved Spectra.....	41
III.	Line vs. Continuum Intensity.....	42

LIST OF ILLUSTRATIONS

Figure		Page
1.	Explosive-driven Shock Tube	7
2.	End Plate for Shock Tube	10
3.	Smear Camera	12
4.	Dispersion Curve for Hilger Medium Quartz Spectrograph	15
5.	Arrangement for Time-integrated Spectra	19
6.	Records from a Time-integrated Shot	21
7.	Arrangement for Time-resolved Spectra	23
8.	Time-resolved Spectra	27
9.	Preliminary Results	31
10.	Densitometry	34
11.	Line Shapes from Fig. 10	36
12.	Shock Velocity Measurements from Transit Times	44
13.	Distance-Time Diagram of Processes in the Explosive-driven Shock Tube	49
14.	Temperature behind the Reflected Shock Wave	53
15.	Electron and Ion Density behind the Reflected Shock Wave	54
16.	Velocity of the Reflected Shock Wave	55
17.	Pressure behind the Reflected Shock Wave	56
18.	Density behind the Reflected Shock Wave	57
19.	Degree of Ionization behind the Reflected Shock Wave	58
20.	Ninety Per Cent Confidence Intervals for $n = 1$ and $n = 3$	59

21. Static Stark Effect, Second Order..... 76

22. Step Approximation to a Dispersion Line Shape..... 77

23. Comparison of Theory (Neglecting Self-absorption) with Experiment..... 80

24. Shift of the Line at 4713 A..... 81

25. Shift of the Line at 5015 A..... 82

26. Effect of Self-absorption on Theoretically Predicted Line Shapes..... 86

27. Depression of Series Limits..... 88

28. Shift of the Line at 6069 A..... 90

29. Shift of the Allowed-Forbidden Pair at 4470 and 4471 A..... 92

THE VISIBLE RADIATION FROM HELIUM IN A STRONG SHOCK WAVE

CHAPTER I

INTRODUCTION

The research described here was performed as a part of the Graduate Thesis Program of the Los Alamos Scientific Laboratory in cooperation with the University of Oklahoma. The problem was therefore chosen on the basis of its mutual interest to the two institutions, and the availability of facilities peculiar to Los Alamos.

The Department of Physics at the University of Oklahoma has, for several years, been actively studying the kinetics, hydrodynamics, and spectra of partially ionized gases produced by electrical spark discharges.[1,2,3] Many questions arise in this work about the behavior of hot gases at equilibrium and how this behavior is related to that in a spark discharge. Thus an investigation of the spectrum of a partially ionized gas in a known equilibrium state would be pertinent to work being done at the University of Oklahoma.

It was felt that facilities at the Los Alamos Scientific Labora-

---

[1] R. Lee and R. Fowler, Phys. Rev. 81, 457 (1951).

[2] R. Fowler, W. Atkinson, and L. Marks, Phys. Rev. 87, 966 (1952).

[3] R. Fowler, W. Atkinson, W. Compton, and R. Lee, Phys. Rev. 88, 137 (1952).

tory might provide samples of a gas at temperatures like those found in sparks and allow the samples to be studied while in known equilibrium states. Unpublished results of earlier experiments at Los Alamos in which an explosive-driven shock wave moved through a tube of stationary gas and was reflected at a rigid wall suggested that the gas in the reflected shock would have a temperature of 1 or 2 ev. It was not known, however, whether sufficient purity could be obtained to allow useful spectrographic studies, or how nearly the gas behind the reflected shock would approach an equilibrium state.

Preliminary shock tube experiments were then made which demonstrated the feasibility of conducting a spectrographic study of partially ionized helium in a known equilibrium state. This problem was of mutual interest to the two sponsoring institutions and its investigation required facilities which were peculiar to Los Alamos. Helium was used because it has a simple structure and is subject to comparatively simple theoretical treatment. The results of such experiments with helium would, however, have been of interest to astrophysicists even in the absence of satisfactory theories.

The visible spectrum of helium both in a strong external electric field and in the presence of ions has been a subject of considerable theoretical interest. Because of its simple structure, the helium atom has often been treated as a perturbed hydrogen atom where the magnitude of the perturbation is determined by the separation of corresponding energy levels in hydrogen and helium. Foster[4], in 1927, applied quantum mechanics to the Stark effect in helium and verified his theoretical

---

[4] J. S. Foster, Proc. Roy. Soc. (London) A117, 137 (1927).

results with experiment. In 1945, Krogdahl[5] considered the effect of the nonhomogeneity of the ionic fields in stellar atmospheres on several helium lines, particularly the forbidden transition 4^3D--2^3P. Huang[6] has studied the shapes and magnitudes of the recombination and photo-ionization coefficients. Most recently, Kivel[7] investigated the effects of the electrons present in partially ionized helium on the shape and shift of the spectral lines and made suggestions for an experimental check of the theory.

In order to compare experimental results with theoretical predictions it was necessary to know the conditions in the emitting gas. Plane wave shock hydrodynamic theory predicts the state of an equilibrated gas behind a shock wave as a function of initial conditions and shock velocity. Here again, helium was a favorable choice because it is normally a monatomic gas, and no vibration, rotation, or dissociation energies appear in the partition function. The validity of the assumption that the gas behind the shock would be equilibrated depended on the relaxation time for electronic excitation and ionization coupled with the rate of radiative and conductive cooling. It was proposed that these features could be studied by familiar smear camera techniques and perhaps by making time-resolved spectra.

If the ability of theory to predict the characteristics of the spectrum of partially ionized helium had been neglected, experimental results would have been useful in providing an empirical relation between

---

[5] M. K. Krogdahl, Astrophys. J. 102, 64 (1945).

[6] S. S. Huang Astrophys. J. 102, 64 (1948).

[7] B. Kivel, Phys. Rev. 98, 1055 (1955).

the state of the emitting gas and the spectrum. Line broadening and shift, strengths of forbidden lines, and relative intensities of lines have long been used to probe conditions in stellar atmospheres and gas discharges. Spectral line broadening and shift and strengths of forbidden lines were to be studied in detail, but the determination of intensities of lines and thus transition probabilities was considered too tedious a task for the initial experiments.

At the time the research for this thesis was begun Kantrowitz[3] and his associates at Cornell University had published results of experiments using argon in a conventional shock tube, and Turner[9] was conducting experiments with hydrogen in the same manner at the University of Michigan. Helium, however, was not amenable to study in a conventional shock tube because of its high ionization potential and high sound speed. The high excitation and ionization potentials of helium necessitate a stronger shock wave than is required for either argon or hydrogen if one is to obtain comparable temperatures and ion densities. Because of the nature of the conventional shock tube, where the shock strength is limited by the ratio of the sound speed in the driver gas to that in the driven gas, helium can be shocked only about one-third as strongly as argon and only slightly more strongly than hydrogen. Replacement of the driver gas and diaphragm of a conventional shock tube with a block of high explosive provided the additional shock strength necessary to permit useful studies

---

[8] H. Petschek, P. Rose, H. Glick, A. Kane, and A. Kantrowitz, J. Appl. Phys. 26, 83 (1955).

[9] E. B. Turner, "The Production of Very High Temperatures in the Shock Tube with an Application to the Study of Spectral Line Broadening," AFOSR TN-56-150, ASTIA Document No. AD 86309 (1956).

of helium to be made. The primary shock wave was reflected at a rigid wall and the light emitted by the helium behind the reflected shock was observed. The Los Alamos Scientific Laboratory was particularly well suited for these experiments, where special explosives, firing facilities, and techniques were required.

This thesis contains a description of the experiments which were made, the results which were obtained, and a comparison of these results with predictions based on some of the available theories. Chapter II is concerned with the apparatus used in the experiments with emphasis on the explosive-driven shock tube and the care necessary in its preparation for use with helium. The way in which the experiments were carried out is treated in Chapter III, where several schematic diagrams are included to clarify the time history of the hydrodynamics, light emission, and operation of the recording instruments. The experimental data are presented in Chapter IV along with the methods and results of data analysis. Chapter V is a discussion of the hydrothermodynamic calculations, and considerable space is allotted to the justification of assumptions implied by the calculational method. Theories which predict the behavior of the visible spectrum of helium are discussed and applied to the experimental conditions in Chapter VI. Of particular interest is a method of predicting spectral line shapes and shifts wherein the effects of perturbations due to ions and electrons are combined in an approximate way with self-absorption broadening to give fair agreement with experiment. The concluding chapter summarizes the work, points out certain improvements which could be made, calls attention to additional problems which have appeared, and suggests methods for their investigation.

CHAPTER II

APPARATUS

Explosive Shock Tube

The explosive shock tube used here may be considered as a conventional shock tube with the driver section and diaphragm replaced by a block of high explosive. The details of the shock tube are shown schematically in Fig. 1. It consisted of a cylindrical Pyrex tube with one end closed by a flat Pyrex plate and the open end sealed to the explosive. A 1/8" diameter hole was located in the side for pumping and filling. The high explosive was also cylindrical in shape. One end was coated with a thin (~0.010") layer of a hard black plastic called Furane Adhesive Type X-2[1] to provide a vacuum tight surface on the explosive and an opaque layer in front of the explosive light. The surface of the Furane was polished flat with grinding compound before being cemented to the Pyrex tube to help in maintaining a plane shock wave. The reasons for requiring a plane wave will be discussed below. The charge was cemented to the end of the Pyrex tube with Armstrong A-1 Cement.[2]

The shock tube just described grew out of several less successful

---

[1]Manufactured by Furane Plastics Incorporated, 719 West Broadway, Glendale 4, California.

[2]Manufactured by Armstrong Products Company, 455 Argonne Road, Warsaw, Indiana.

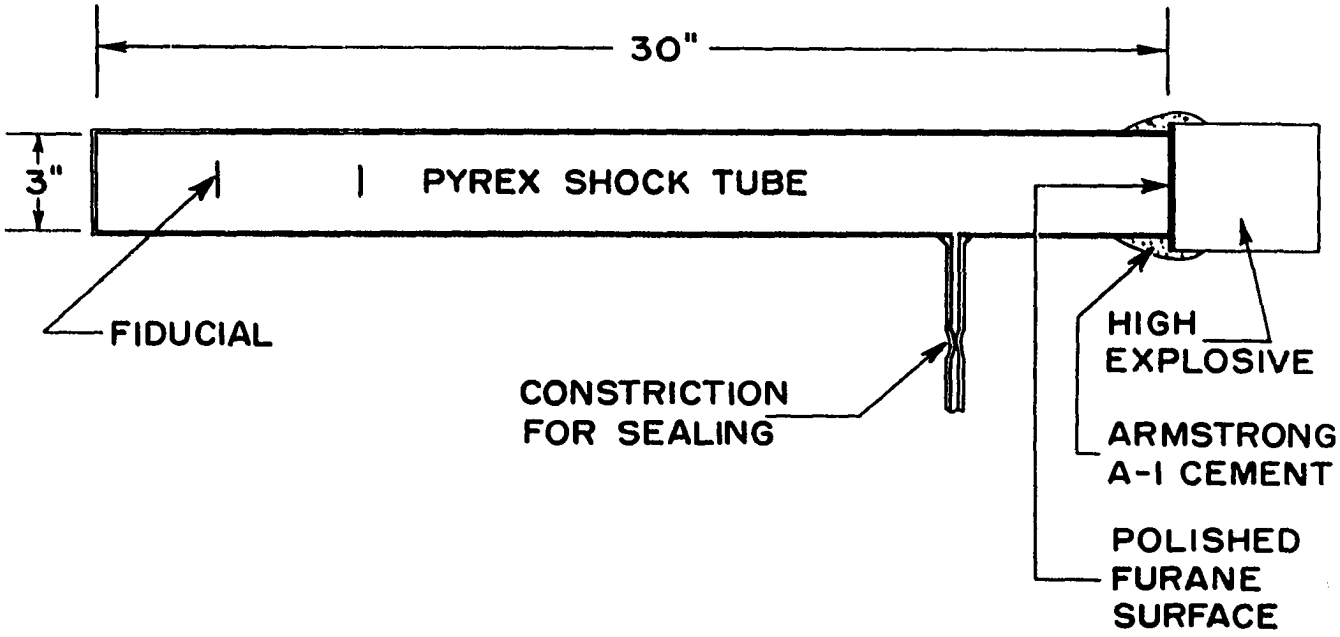

Fig. 1. The Explosive-driven Shock Tube

designs. It was found that the following requirements have to be satisfied in an acceptable tube design:

(1) The tube must hold a vacuum of about 10^{-5} mm Hg; otherwise, easily excited impurity lines contribute significantly to the observed spectrum. This is qualitatively reasonable when it is recalled that the first excited state of helium is at about 20 ev, whereas elements like sodium and calcium are ionized with 5.14 and 6.11 ev respectively.

(2) The shock wave must be plane, primarily because plane shock wave hydrodynamic theory was used to calculate the thermodynamic state of the gas behind the reflected shock wave. Also nonplanar waves were always accompanied by seriously contaminated spectra, probably due to excessive mixing between the expanding explosive products and the hot compressed helium.

To obtain a high vacuum in the shock tube before filling, it was necessary to separate the explosive surface from the evacuated region. Best results were obtained when the explosive surface was coated with Furane. Glyptal was also used, but resulting spectra were contaminated with impurity lines. The tube could be cleaned even more thoroughly by using glass or quartz tubes with flat plates sealed on both ends such that the entire tube could be baked during pumping. As expected, higher vacua were obtained, but when high explosive was butted against one end and fired a nonplanar wave resulted, accompanied by a highly contaminated spectrum.

The diameter of the tube was somewhat arbitrary above a minimum value where the boundary layer effects were great enough to cause observable deviations from planarity in the wave. This minimum diameter was somewhere between 1" and $2\frac{1}{2}$". Also, clearly, the bigger the tube the more light produced per unit area normal to the axis of the tube.

The construction of the closed end of the tube depended on the method of observing the spectrum. For time-integrated spectra the Pyrex end plate was sealed on by a glassblower and observations were made through this flat surface. Time-resolved spectra, however, were observed through the cylindrical surface near the closed end, and distortion caused by blowing the glass in this region could not be tolerated. In this case, the end plate was cut as shown in Fig. 2 and cemented to the cylinder with Armstrong A-1 Cement.

The tube-explosive assembly was sealed to a glass high-vacuum system which could be evacuated to about 10^{-7} mm Hg. This system consisted of a mercury diffusion pump and forepump with three cold traps advantageously located. A glass bulb of spectroscopically pure helium was also sealed to the system in such a manner that the helium passed through two of the liquid-nitrogen-cooled traps on its way to the shock tube. The shock tube was evacuated to about 10^{-6} mm Hg, baked at about 300°C in regions remote from the explosive, flushed and evacuated again, filled to the desired pressure, and sealed off at the constriction shown in Fig. 1.

Smear Camera

Shock wave velocities and shapes were observed with a rotating mirror type smear camera. The operation of the camera is shown schemati-

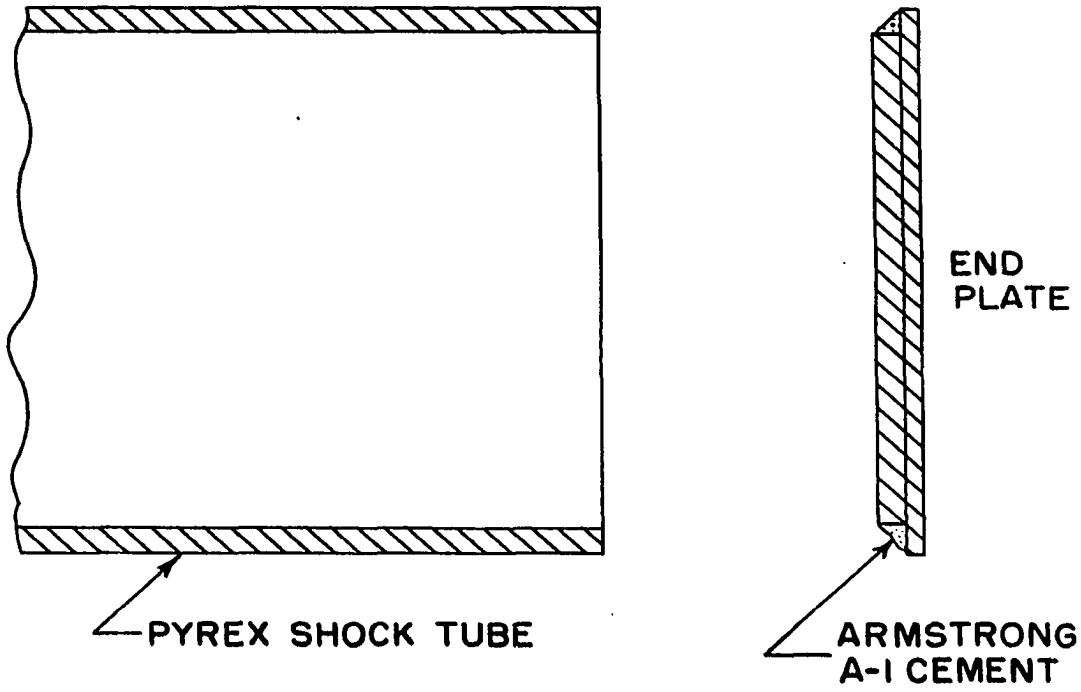

Fig. 2. End Plate for Shock Tube

cally in Fig. 3. Light from the object to be photographed is focused in the plane of the slit. The camera lens and rotating mirror relay an image of the slit onto the film plane, and this image is swept across the film plane by the rotating mirror. In this manner the light passing through the slit is recorded as a function of time. If, for example, the image of a light producing phenomenon moves along the slit the resulting record will show a plot of position versus time, thus giving a measure of velocity.

A Model 74, f/4, 7" writing arm camera, built by the Optics Group at LASL, was used. The rotating mirror was driven by an air turbine capable of operation at speeds up to 1600 rps. Speeds between 300 and 600 rps, giving image speeds from 0.67 to 1.34 mm/μsec, were used in this work. The width of the image of the camera slit on the film was about 0.05 mm so that at 1.34 mm/μsec it smeared about 0.04 μsec over its width.

Since the camera could write for less than one-eighteenth of each revolution, it was equipped with a synchronizer which permitted a firing circuit for the explosive to be pulsed at the proper position of the mirror. A small tilted reflecting surface on the end of the rotating mirror shaft relayed a beam of light from a source to a photomultiplier tube when the mirror was in a given position. The output of the photomultiplier triggered a thyratron in a gating circuit only after the firing switch had been closed. Thus, the explosive firing circuit was pulsed by the first pulse from the photomultiplier after the switch was closed. The delay between the firing pulse and the time at which the camera began writing was controlled by rotating the source and photomultiplier system about the axis of the rotating mirror and locking it at the proper angle.

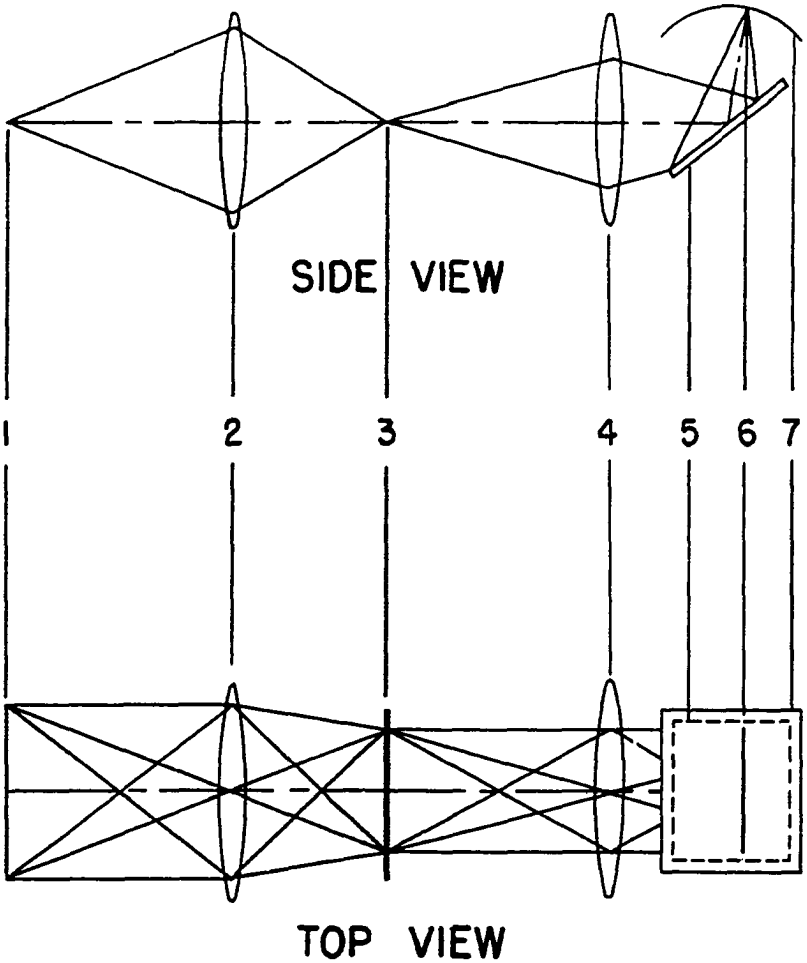

1. OBJECT
2. OBJECTIVE LENS
3. SLIT
4. CAMERA LENS
5. ROTATING MIRROR
6. IMAGE
7. FILM PLANE

Fig. 3. Smear Camera

Smoke Shutter and Monitor

A Primacord smoke shutter was used to interrupt the passage of light to the spectrograph shortly (~10 μsec) after shock wave reflection time. This was necessary to prevent light emitted at later times with gas in an unknown state from being recorded on the spectrogram. The smoke shutter consisted of a circle of Primacord explosive fuse placed on the face of a plane relay mirror at a safe distance from the spectrograph. Shortly after the Primacord was detonated a cloud of dense smoke obstructed the passage of light to and from the mirror. Before the smoke had cleared, the mirror had been shattered, thus permanently shuttering the spectrograph.

The length of time during which the helium light exposed the spectrographic plate was about 10 μsec, beginning about 100 μsec after the explosive was detonated.

The firing pulse for the shutter was controlled by the settings of the camera synchronizer and a phantastron delay circuit. A pulse from the synchronizer was split so as to feed both the firing circuit for the shock tube explosive and the phantastron. The shutter firing circuit received a pulse from the phantastron after an appropriate time delay which corresponded to the sum of the explosive transit time, the shock tube transit time, and the lifetime of the reflected shock wave diminished by the inherent delay of the shutter.

Operation of the smoke shutter was monitored by a photomultiplier positioned so that it recorded the light from a sample taken from the beam entering the spectrograph. In this manner a permanent record of the operation of the shutter was obtained on an oscillogram.

Spectrograph

A Hilger Medium Quartz Prism Spectrograph was used throughout these experiments. The effective aperture of the instrument was about f/16. Its dispersion curve is shown in Fig. 4.

An f/8 parabolic mirror formed an image of the region being studied on the slit of the spectrograph. A reasonably stigmatic image was necessary if time-resolved spectra were to be made, and desirable even for time-integrated spectra. This will become clear in a later chapter when these two methods are treated separately in detail.

The spectrograph was equipped with a solenoid-operated shutter which opened when the "fire" switch was depressed, thus admitting scattered daylight for only a few seconds. This was adequate to prevent fogging of the plate since more than 2 min of daylight were required to produce damaging fog.

Electrodeless Discharge

An electrodeless discharge was used to place helium reference spectra on each spectrogram. This permitted a direct measurement of line shift and provided spectrograph dispersion-curve data on each plate. A spectroscopically pure helium sample for the electrodeless discharge was held in a quartz tube about 3" long and 3/8" in diameter. The tube was evacuated to a pressure of about 10^{-7} mm Hg and flamed to a red heat before being filled with helium to a pressure of 10 mm Hg. The sample was excited by microwaves from a commercial Microtherm diathermy machine.

Photographic Material

Eastman Tri-X Panchromatic Film was used in the smear camera in

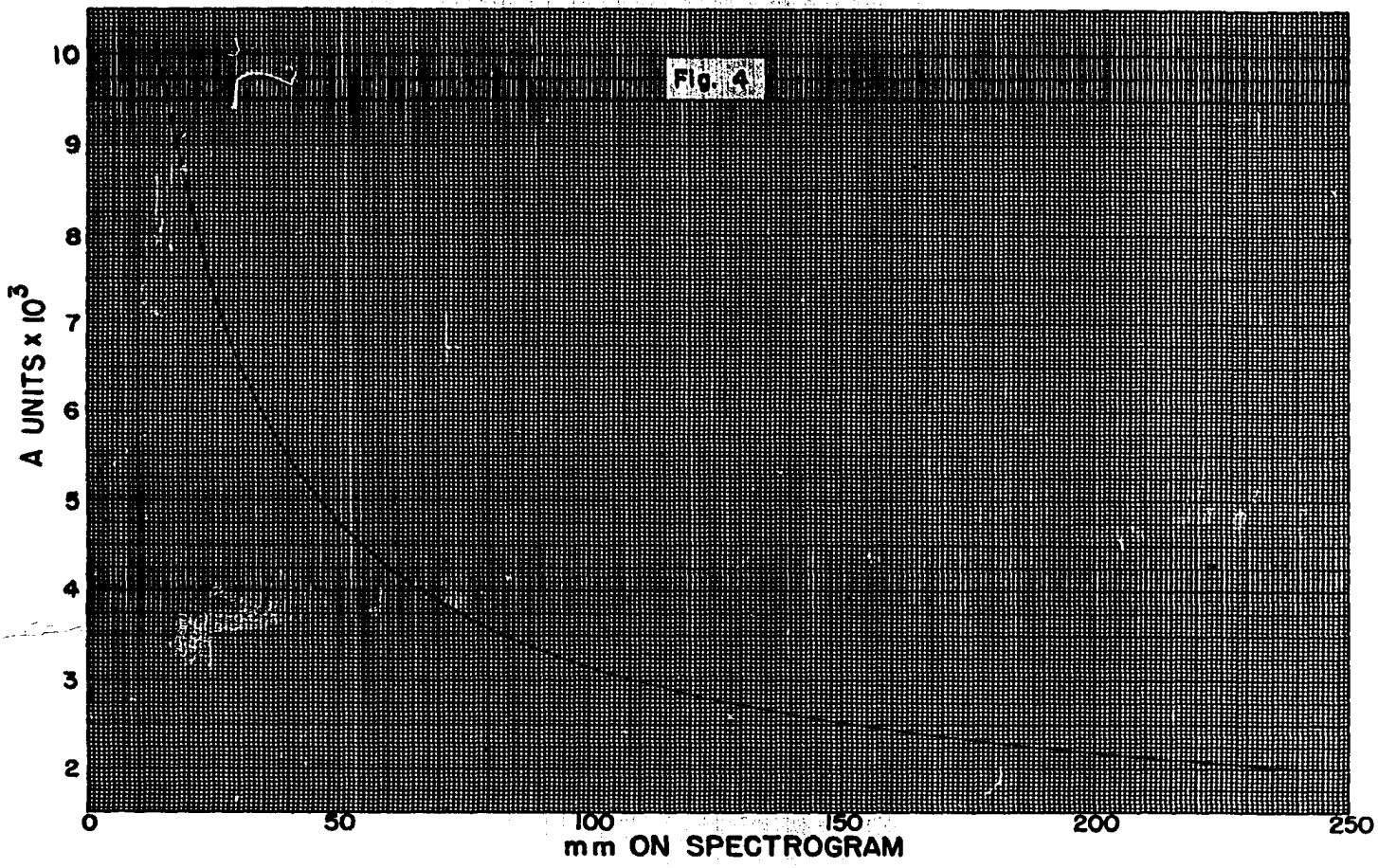

Fig. 4. Dispersion Curve for Hilger Medium Quartz Spectrograph

early experiments, and later it was replaced by a faster film, Eastman Royal Pan. These films were developed for 4 min in Eastman Rapid X-Ray Developer.

Eastman Tri-X Panchromatic Type B Plates were used in the spectrograph because of their high speed and fairly flat response over the visible portion of the spectrum. Also, this emulsion is not subject to significant failure of the reciprocity law for times of 1 μsec or greater. In an attempt to retain as much speed as possible and at the same time improve resolution, the plates were brush developed in Eastman D-19 for 8 min. A plate with less granularity would certainly have been more desirable but any such plate would not have had the requisite speed for the small amount of light available.

CHAPTER III

EXPERIMENTAL ARRANGEMENTS AND PROCEDURES

When this work was begun it was not known whether sufficient light could be gathered from helium to expose a spectrogram. Thus the first experiments were designed to integrate the useful light over time on the spectrogram. Qualitatively, spectra obtained in this manner were as expected with regard to line broadening and shift, forbidden lines, etc., but a quantitative comparison of these results with theoretical predictions required the assumption that most of the light was emitted during a period when the gas behind the reflected shock wave was in a constant state of kinetic equilibrium. Kinetic equilibrium, as used here, differs from thermodynamic equilibrium by the absence of radiation equilibrium.

Deviations from kinetic equilibrium due to excessively long relaxation times and radiative cooling could be observed on a time-resolved spectrum, and if a sufficiently dark plate could be obtained it would contain all of the information formerly obtained from a time-integrated spectrum. For initial pressures below 10 mm Hg the film density was marginal, but for higher pressures it was clear that enough light was available to produce a usable film density after an exposure time of 1 μsec. One microsecond corresponded to about one-tenth of the

time during which a clean reflected wave persisted. Thus gross deviations from a constant radiation state would be observable if a time-resolved spectrum could be made with a resolving time of about 1 μsec.

The experiments which gave time-integrated and time-resolved spectra were conducted differently and they will be treated separately here, although many of the data will be combined in a later chapter.

Time-integrated Spectra

Figure 5 shows schematically the arrangement of apparatus for the time-integrated spectra. The cross-hatched region represents the walls of a reinforced concrete building which housed the smear camera, oscilloscope, electronic control circuits, and the operators. The smear camera recorded the shape and velocity of the shock wave. The spectrum was observed from an oblique angle so that the flat end of the tube could be used as a window without exposing the spectrographic plate to light from the entire length of the tube. Shortly before the reflected wave collided with the mixing zone, the Primacord shutter was detonated in order to stop the further passage of light to the spectrograph. It had been shown experimentally that the light emitted by the primary wave in the region seen by the spectrograph was not detectable on a spectrogram; thus, proper operation of the shutter guaranteed that only the light from the reflected shock wave would be recorded.

The parabolic mirror formed an image of the end of the shock tube on both the spectrograph slit and the cathode of the photomultiplier tube. The plane mirror used to reflect a sample of light to the photomultiplier was small enough so that its presence did not appreciably reduce the intensity at the spectrograph.

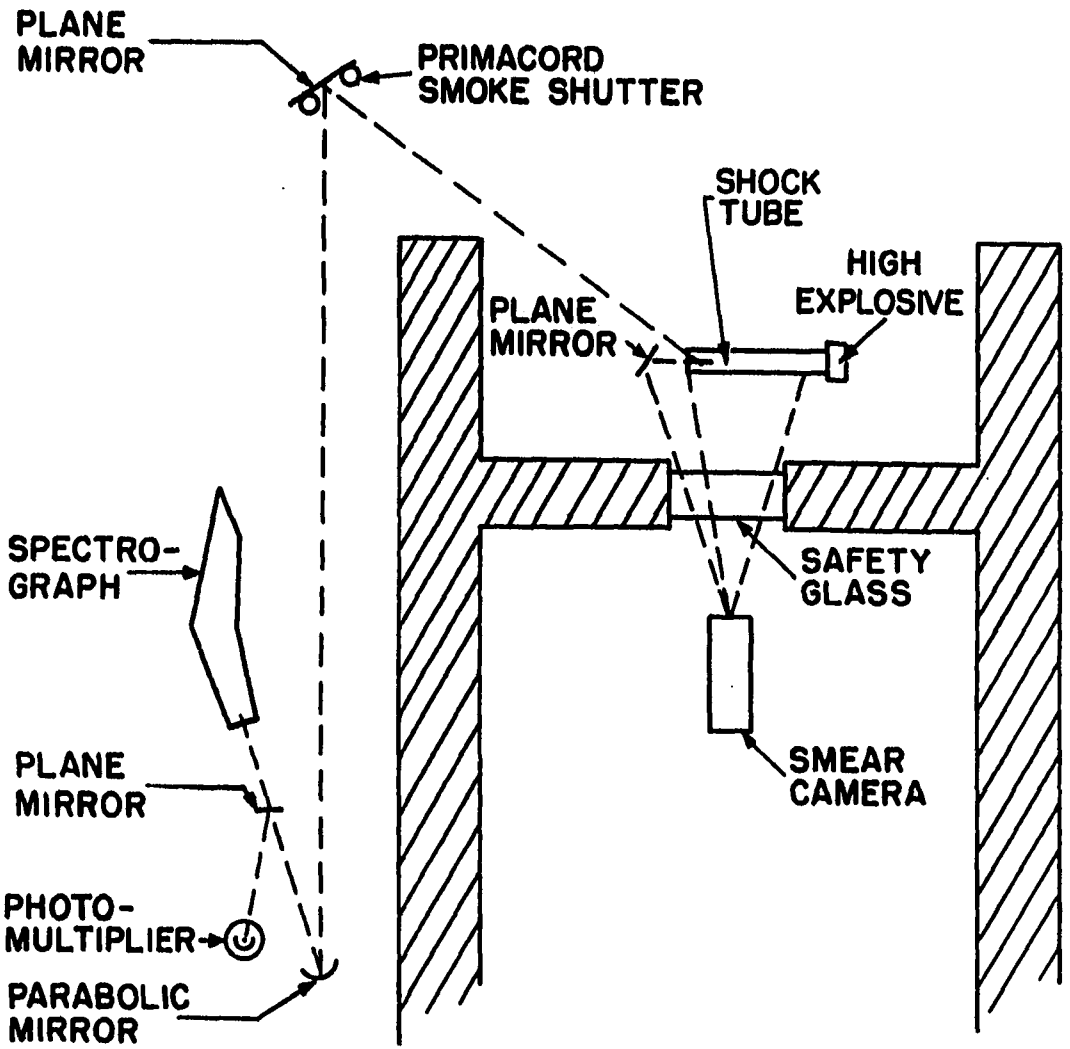

Fig. 5. Arrangement for Time-integrated Spectra

Filled to the desired pressure with helium and sealed, the shock tube was aligned so that its axis was imaged on the slit of the smear camera. The small plane mirror at the end of the tube was then adjusted so that the images of the two ends of the tube appeared as concentric circles in the plane of the camera slit.

Alignment of the spectrograph with the mirrors in the spectrograph beam was accomplished by placing an ordinary incandescent lamp near the film plane of the spectrograph. This permitted a beam to be directed through the spectrograph onto the parabolic mirror, the smoke shutter relay mirror, and the shock tube. Then the end of the shock tube was illuminated and its image was focused on the plane of the spectrograph slit by adjusting the relay mirror, alignment always being maintained by use of the light source in the film plane. The photomultiplier was then adjusted so that the image of the end of the tube was focused on its photocathode.

Proper timing of the events during a shot required prior knowledge of shock velocities, transit times of the various explosive components, and the inherent delay in the smoke shutter. Camera speed was adjusted so that the angle θ in Fig. 6 would be about 45° for best reading accuracy, while the synchronizer was adjusted so that the camera would be "writing" while the shock wave proceeded down the tube and was reflected. More precise values of shock velocities and transit times along with inherent shutter delay were required in order to adjust a phantastron delay circuit so that the smoke shutter would close at the proper time. Shock velocities and transit times were estimated roughly, then measured in preliminary experiments. Inherent delay in the shutter

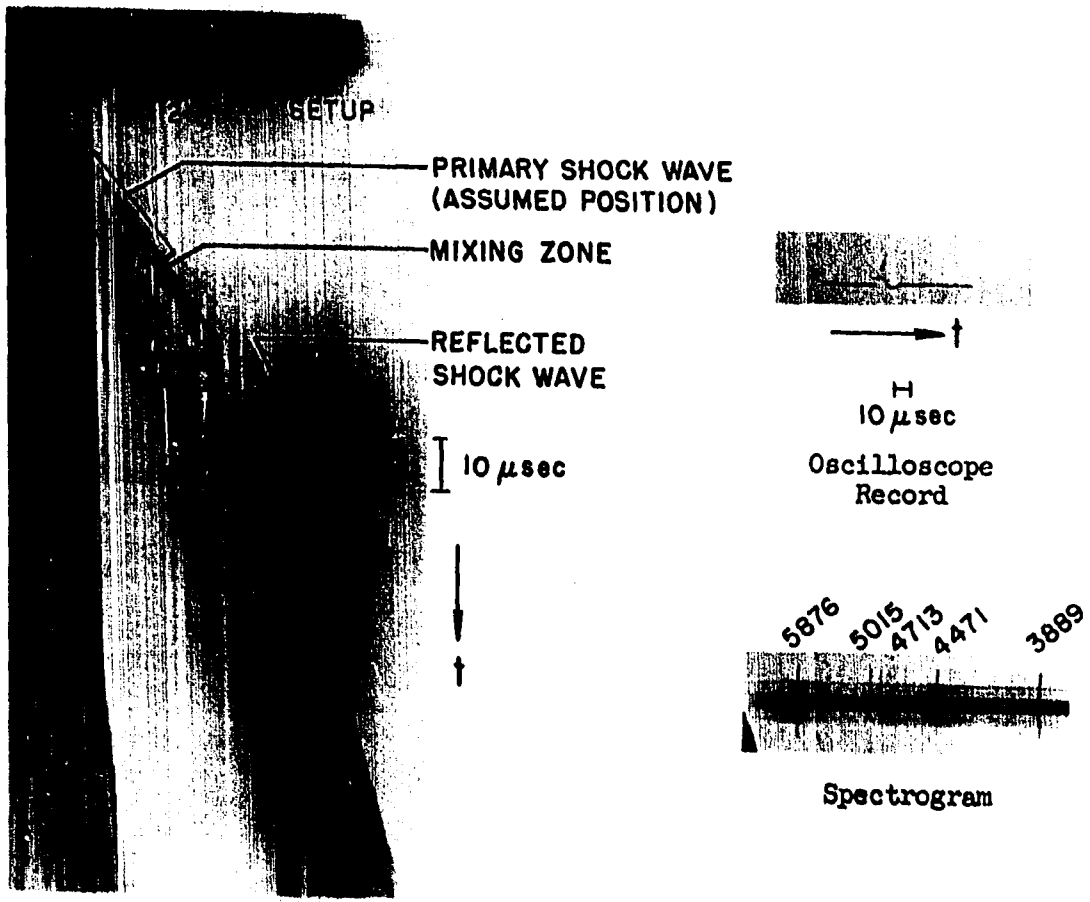

Fig. 6. Records from a Time-integrated Shot

was measured by observing shutter operation with the smear camera when a bursting wire was used as a light source.

When a shot had been aligned and the synchronizer and phantastron had been adjusted, the slide in the spectrograph cassette was pulled and the spectrographic plate was exposed to the helium reference spectrum in regions above and below the space which was to be exposed during the shot.

All preparations having been made, the shot was fired and the resulting plate and films were developed.

An example of satisfactory records made during a shot is shown in Fig. 6.

Time-resolved Spectra

The arrangement of apparatus for producing time-resolved spectra is shown in Fig. 7. With the rotating mirror in the position shown, an image of the shock tube slit was formed on the spectrograph slit (Section CC), and a narrow spectrum thus formed in the film plane of the spectrograph. As the rotating mirror turned (Section BB) the position of the spectrum moved a proportional amount down the spectrograph slit, and changes in a stationary light source near the end of the shock tube slit could be recorded on a spectrogram as a function of time.

Like the smear camera, the spectrograph could write for only a small portion of each revolution of the mirror, and it was necessary to synchronize the explosive firing time with the position of the mirror. In this case the synchronizer was adjusted so that the spectrograph would begin "writing" shortly before the primary shock wave reached the end of the tube. The operating speed of the mirror was chosen so that a spectrogram would include about 15 μsec, whereas the lifetime of the

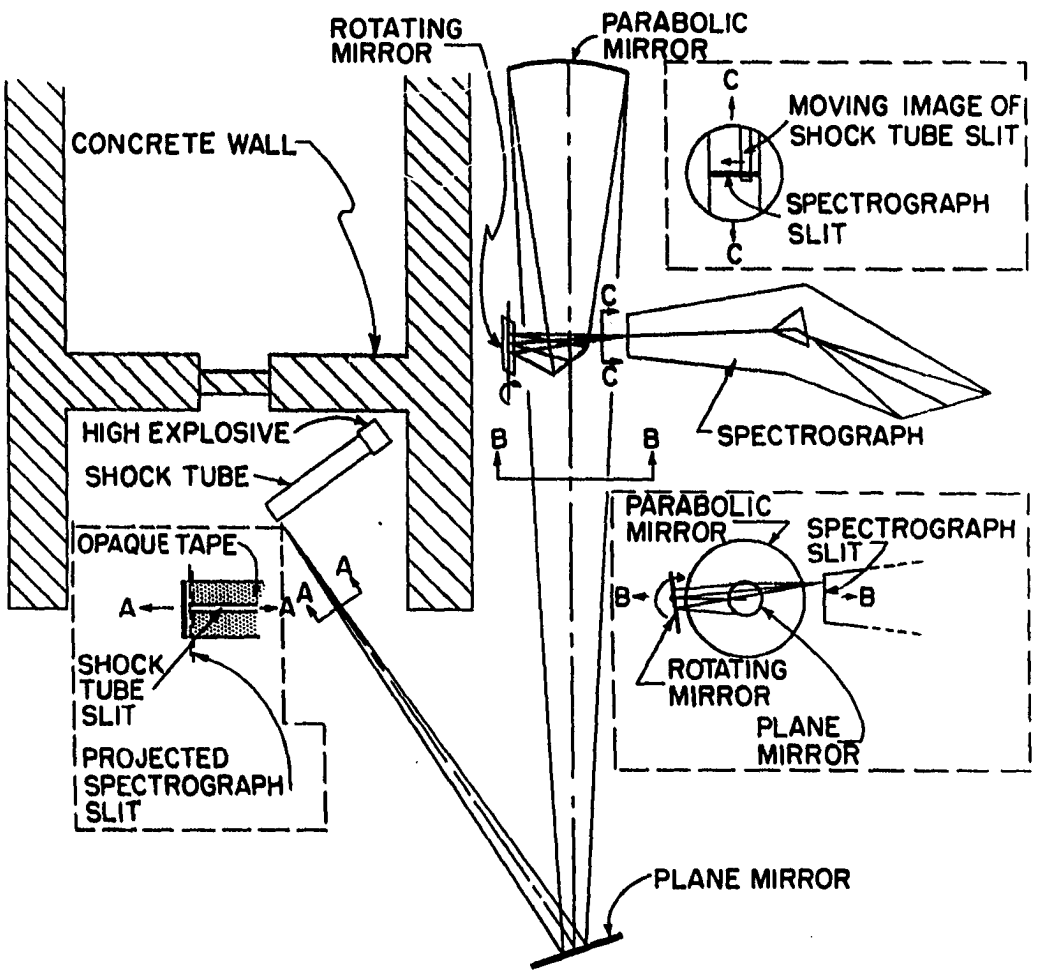

Fig. 7. Arrangement for Time-resolved Spectra

reflected shock wave was about 10 μsec. Because of jitter in the synchronizer mechanism only about one-half of the shots fired in this way gave a full time history of the reflected shock wave. The region to be viewed by the spectrograph (intersection of projected spectrograph slit and shock tube slit in Fig. 7, Section AA) was located as near to the end of the shock tube as seemed practical -- a small separation was thought necessary to exclude light which might be emitted at the surface of the reflecting Pyrex end plate.

The total response time of this system will be defined as the time required for the intensity at the spectrogram to rise to full value if an intensity step function moves across the spectrograph slit. This time response may be conveniently divided into two parts: (1) the effect of the shock tube slit width and rotating mirror speed, and (2) the effect of the spectrograph slit width and the speed with which the step function moves.

First, assume that the shock tube slit area becomes suddenly illuminated uniformly. Clearly the ability to follow such a light change is proportional to the width of the shock tube slit. The length of time, T_t, for the total light falling on any point on the photographic plate to reach its maximum value is equal to the length of time required for the image to sweep its own width. This can be expressed by

$$T_t = \frac{W_{ti}}{S} = \frac{W_t}{M2\omega a}$$

where W_t = width of shock tube slit

$$M = \frac{\text{parabolic mirror to shock tube distance}}{\text{parabolic mirror to spectrograph slit distance}}$$

ω = angular velocity of rotating mirror

$W_{ti} = W_t/M$ = width of image of shock tube slit

a = writing arm (mirror to slit distance)

$S = 2\omega a$ = writing speed

For a typical set of numbers T_t = 1.2 μsec.

Now consider the case in which the mirror is not moving but a discontinuous intensity step function travels down the shock tube. Here the intensity at the spectrogram will rise during the time, T_s, required for the step function to travel across the image of the spectrograph slit projected into the shock tube. There is also a correction for the effective spreading of the slit due to the depth of the light source in the shock tube. For this case

$$T_s = \frac{0.07 \text{ mm} + W_s}{D/M}$$

where W_s = spectrograph slit width

D = reflected shock velocity (step function velocity)

0.07 = effective spreading of slit (mm)

A typical set of numbers yields T_s = 0.2 μsec. The total response time of the system is $T_t + T_s = T$.

In order to align the system shown in Fig. 7, a beam of light from a source placed in the film plane of the spectrograph was centered in all of the mirrors successively then the shock tube was moved into place as shown in the sketch. The system was focused by illuminating the shock tube slit and adjusting the relay mirror while maintaining alignment. The axis of the shock tube was made perpendicular to the light beam by placing a plane mirror flush against the side of the shock tube and forcing the light beam to retrace itself.

Prior to each shot, helium reference spectra were placed at the top, center, and bottom of the spectrogram. These were about 1/2 mm wide, corresponding to about 1/2 μsec in writing time. This caused at least one reference spectrum to be superimposed on a small portion of the spectrum from the helium in the reflected shock wave. Some time-resolved spectra are presented in Fig. 8. The response time in Fig. 8(a) is 1/2 μsec, and it is clear that equilibrium was not reached in the first 1/2 μsec after the passage of the shock wave for initial pressure less than 20 mm Hg. There is no indication of significant radiative cooling, i.e., a steady radiation state seems to persist until the reflected shock wave collides with the mixing zone. Fig. 8(b) presents spectra wherein the response time was lengthened for the purpose of obtaining darker spectra for quantitative analysis.

Shock velocity measurements were not made simultaneously with the time-resolved spectra. To do this would have required either the use of a continuously writing smear camera, which was not at hand, or synchronization of the two air-turbine-driven rotating mirrors, one in the smear camera and one for time-resolving the spectrum. Consequently, velocities were measured on several shock tubes which were apparently identical to those used for obtaining the time-resolved spectra to which the velocities were applied.

Much difficulty had been encountered in making accurate measurements on the slope of the shock line (Fig. 6) on films made with time-integrated spectra, and a more precise method for measuring velocity was sought for use with the time-resolved spectra. While investigating methods for measuring shock velocity, it was noticed that by using

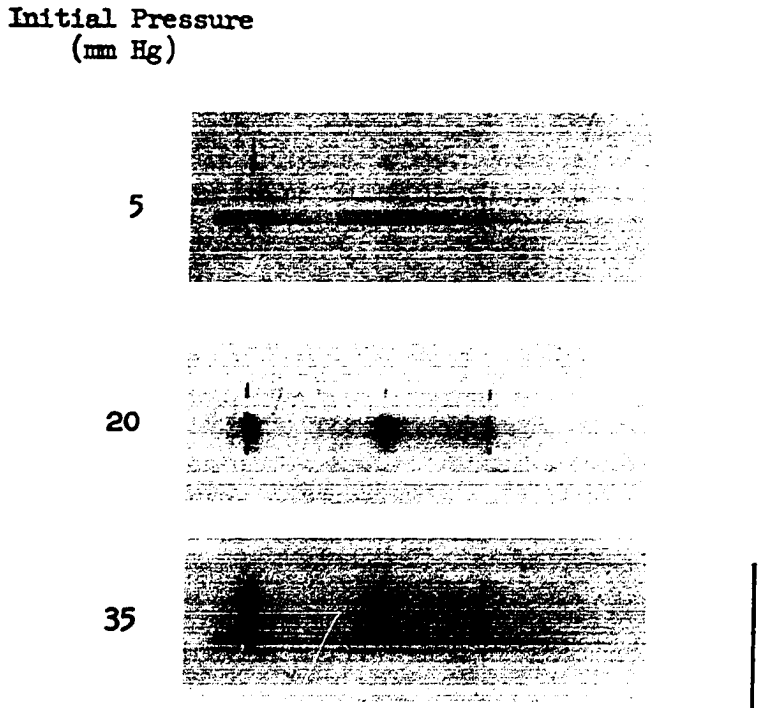

Fig. 8. Time-resolved Spectra

Eastman Royal Pan Film, an accurate measurement of shock tube transit time could be made if the smear camera synchronizer were set to record, in addition to the reflection, the time at which the shock wave entered the helium. This, of course, only gave a value of average shock velocity, but it was shown that the average velocity in a tube 10" long was, within experimental error, the same as that in a tube 30" long. These data, which led to the assumption of constant shock velocity, are treated in a later section.

Two unsuccessful attempts were made to measure the position of the primary shock wave at several points as a function of time. The first was a shadowgraph method, in which a grid placed next to the shock tube on the side opposite the camera was illuminated by an argon flash.[1] It was hoped that the shock front would be dense enough to absorb a detectable amount of the argon light or cause a sudden curvature in the elements of the grid as seen through the shock wave, but neither effect was observed. The other vain effort consisted of placing thin barriers along the inner surface of the shock tube, hoping to see minute reflections which would be so small as not to disturb the plane wave hydrodynamics, but in this case also no disturbance was detectable with the smear camera.

Spectrographic Plate Calibration

Measurements of the shape (intensity vs. wavelength) of a spectral line from a spectrogram required that the photographic emulsion be calibrated with respect to relative light intensity in the spectral

---

[1] R. G. Shreffler and R. H. Christian, J. Appl. Phys. 25, 324 (1954).

vicinity of the line. This required a source with which the intensity could be varied in a known way and which emitted continuous radiation, at least in the vicinity of the interesting helium lines. The calibration plates which were used for all of the quantitative measurements were obtained with a 7-step filter,[2] the spectrograph, and an XP-2 xenon flash lamp.[3] The spectrum was continuous with several lines superimposed on it, but the lines were not located in the vicinity of interesting helium lines. The flash lamp was operated with 0.6 μfd at 2000 v.

A calibration was placed on many of the plates which were used for shock spectra with the 7-step filter and a photoflood lamp. This procedure was satisfactory for wavelengths of 4000 A or greater but not for shorter wavelengths because the radiation was absorbed by the glass envelope of the source. These calibrations, however, showed that variations between individual plates were negligible. It was also necessary to know how the response of the emulsion varied with exposure time, i.e., whether the reciprocity law was obeyed. Experiments performed at LASL show a negligible reciprocity failure for times greater than a microsecond.

---

[2] Purchased from the Jarrel-Ash Company, Newtonville, Mass. Rhodium evaporated on crystal quartz. Each step was 1.2 mm wide and the density steps were approximately 0.2. The density range was from 0 (clear quartz) to 1.2.

[3] Purchased from Edgerton, Germeshausen, and Grier. This is a capillary discharge with a 1.2 mm diameter Vycor casing and tungsten electrodes spaced 6 mm apart.

CHAPTER IV

DATA AND ANALYSIS

Qualitative Data

During the development of satisfactory techniques for producing a relatively pure helium spectrum, much of the analysis consisted of visual inspection of spectrograms and smear camera photographs. The spectrograms often were underexposed, overexposed, and/or filled with impurity lines and bands. However, even on some of these plates it was clear that helium line broadening and shift would be measurable quantities and that lines appeared at wavelengths of forbidden helium transitions which had been observed by astrophysicists. The smear camera photographs often showed nonplanar or inclined shock waves, a bright shock line followed by a lightly exposed region, or a thick mixing zone.

Examples of these preliminary data are shown in Fig. 9 and compared to the type of data which was later used for quantitative study.

On Fig. 9(a) the shock wave is plane and a well-defined shock line appears, but several impurity lines are present in the spectrum. Fig. 9(b) shows a nonplaner shock wave followed by a thick mixing zone, again giving a contaminated spectrum. These unsatisfactory results are to be compared with Fig. 9(c), where a clean helium spectrum was obtained. The shock wave is followed by a narrow mixing zone and no shock line

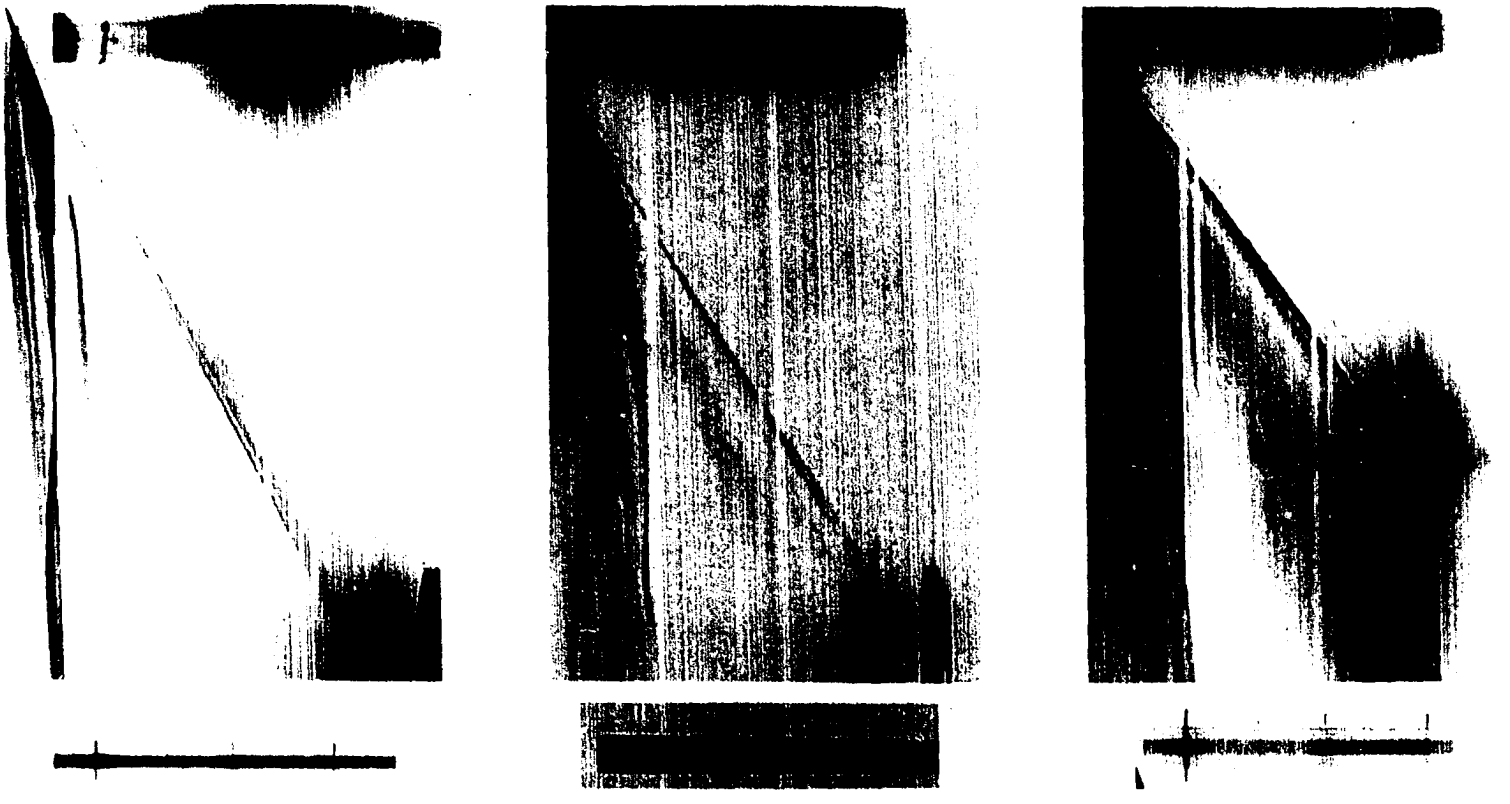

(a)

Dirty Shock Tube,
Plane Wave

(b)

Clean Shock Tube,
Nonplanar Wave

(c)

Clean Shock Tube,
Plane Wave

Fig. 9. Preliminary Results

is observable -- the assumed position of the shock line in Fig. 9(c) was marked by a scratch on the film. The absence of a shock line is in agreement with Turner's[1] conclusion that the shock line in his argon experiment was due to light from easily excited impurity materials. Figure 9(a) demonstrates the necessity of an initially clean shock tube and Fig. 9(b) the necessity of a plane wave.

The phrase "clean helium spectrum" was used in the previous paragraph to describe a case where H_α and H_β were clearly present. These lines persisted in all cases, but because of their wavelengths and low intensities they were not detrimental to the experiments.

Spectrograms

Time-integrated Spectra

All detailed analyses of spectrograms were made on traces from a recording microphotometer. In the case of time-integrated spectra three traces were usually made from a plate: the "shock" trace along the center of the shock tube image, the "reference" trace along the nearest reference spectrum, and the "half and half" trace, which included a portion of the above two regions. The reference trace provided data for a spectrograph dispersion curve which could be plotted directly on the trace, and the half and half trace made it possible to locate the reference trace and dispersion curve with respect to the shock trace.

Without changing the sensitivity or focus of the microphotometer, traces were made at various wavelengths from a step-wedge calibration

---

[1]E. B. Turner, "The Production of Very High Temperatures in the Shock Tube with an application to the Study of Spectral Line Broadening," AFOSR TN-56-150, ASTIA Document No. AD-86309 (1956).

plate. This provided a direct relationship between chart reading and relative exposure on the plate.

The calibration procedure used here gave only relative values and no effort was made to obtain absolute measures of source intensities. It was shown that plots of relative source intensity vs. chart reading made for several wavelengths were the same shape for as much as 100 A on either side of a line. Then, if the emulsion speed was assumed constant over this width and if the chart reading was multiplied at each wavelength by the reciprocal of the slope of the dispersion curve, an intensity profile in the vicinity of a line could be plotted.

Figure 10 shows a print of a spectrogram and the microphotometer traces used in its analysis. Relative sizes here are greatly distorted for purposes of comparison. The actual length of the spectrogram between 3889 and 5876 A was 3.3 cm, whereas, that of the traces was about 125 cm. From the traces it is apparent that the granularity of the photographic emulsion limited resolution, but in most cases the reduced speed of a less granular emulsion would not have produced a measurable film density.

As shown in Fig. 10, the allowed helium lines at 3889, 4471, 4713, 5015, and 5876 A appear on the shock spectrum. Also, two forbidden lines are seen: 4^3F--2^3P at 4470 A and 3^3P--2^3P at 6069 A. Whether certain of the lines were suitable for broadening and/or shift measurements depended on the initial pressure of helium in the shock tube. In the spectrum shown in Fig. 10, shift measurements were made on the lines at 3889, 4470, 4471, 4713, 5015, and 6069 A, and the lines at 3889 and 5876 A were analyzed for shape. The line at 6678 A was not studied in detail because the sensitivity of the photographic emulsion changes rapidly with

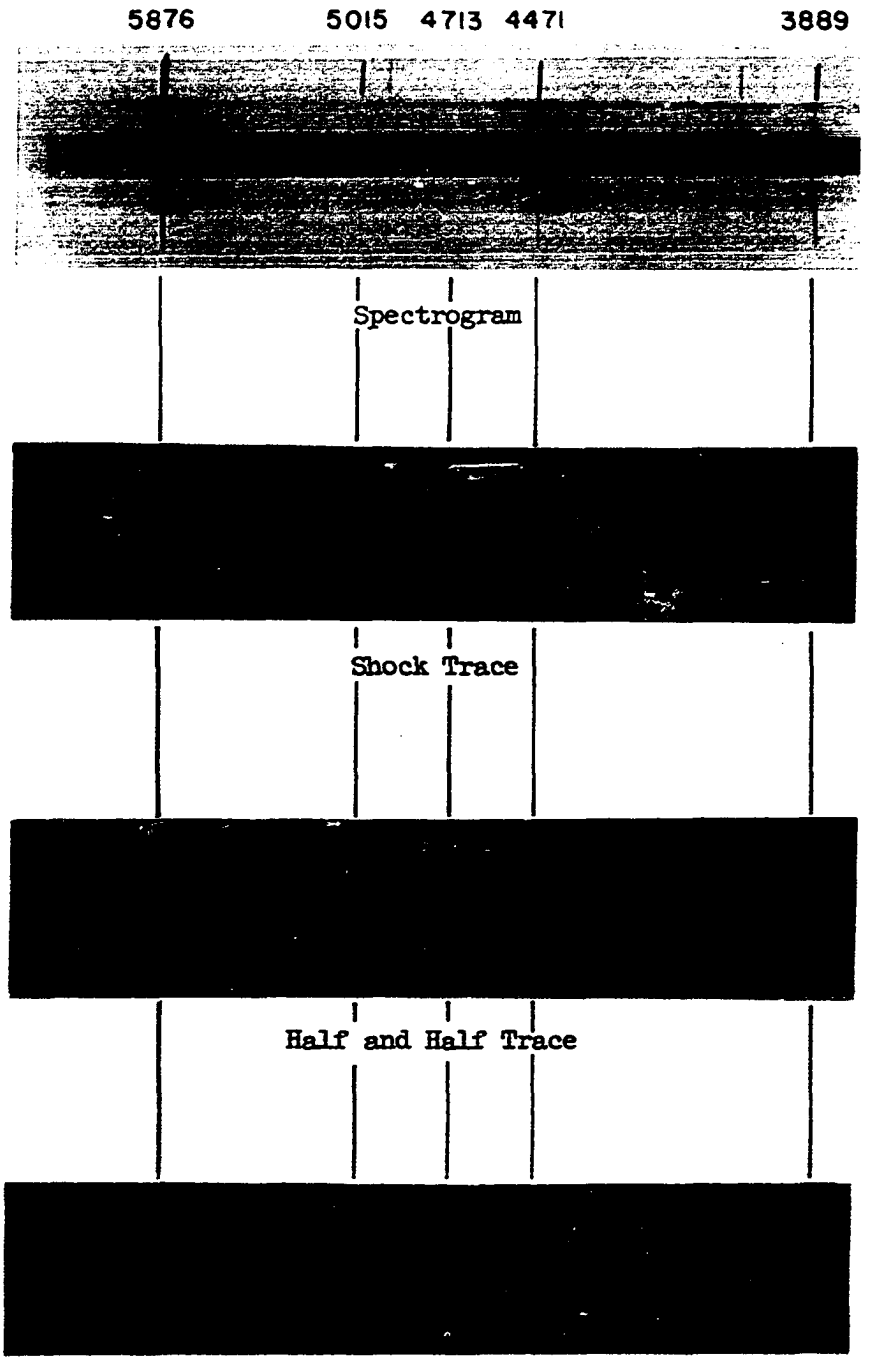

Fig. 10. Densitometry

wavelength in this region of the spectrum.

Line shifts were measured by superposing the reference trace on the shock trace and reading the wavelength of the shifted line from the dispersion curve. The major uncertainty in line shift measurements from a given plate was the location of the center of the shifted line, particularly if the line were broadened asymmetrically. Estimates of the precision of the shift measurements were based on the author's judgment.

The shape (relative intensity vs. wavelength) of a spectral line was obtained as follows: The chart reading was transformed to a function which was proportional to the light intensity on the spectrogram by using the emulsion calibration curve for the wavelength region of the line in question. The spectral response of the emulsion was assumed constant and equal to its value at the line center for the wavelength range of interest on both sides of the line. Since the transmissivities of the quartz elements in the spectrograph and the Pyrex shock tube are essentially constant from 3600 to 6500 A, a function which is proportional to light intensity at the spectrogram is also proportional to intensity at the helium source within the shock tube. Call this function I_x, where x is a linear measure along the spectrogram or microphotometer trace. If I_λ is proportional to the energy, E, per angstrom unit incident on the spectrogram then $I_\lambda = I_x/S$ where S is the slope of the dispersion curve, i.e., $S = d\lambda/dx$.

Line shapes obtained from the spectrogram in Fig. 10 are shown in Fig. 11. It will be shown later that the maximum marked "forbidden" corresponds to the shifted position of the helium forbidden transition 3^3P--2^3P.

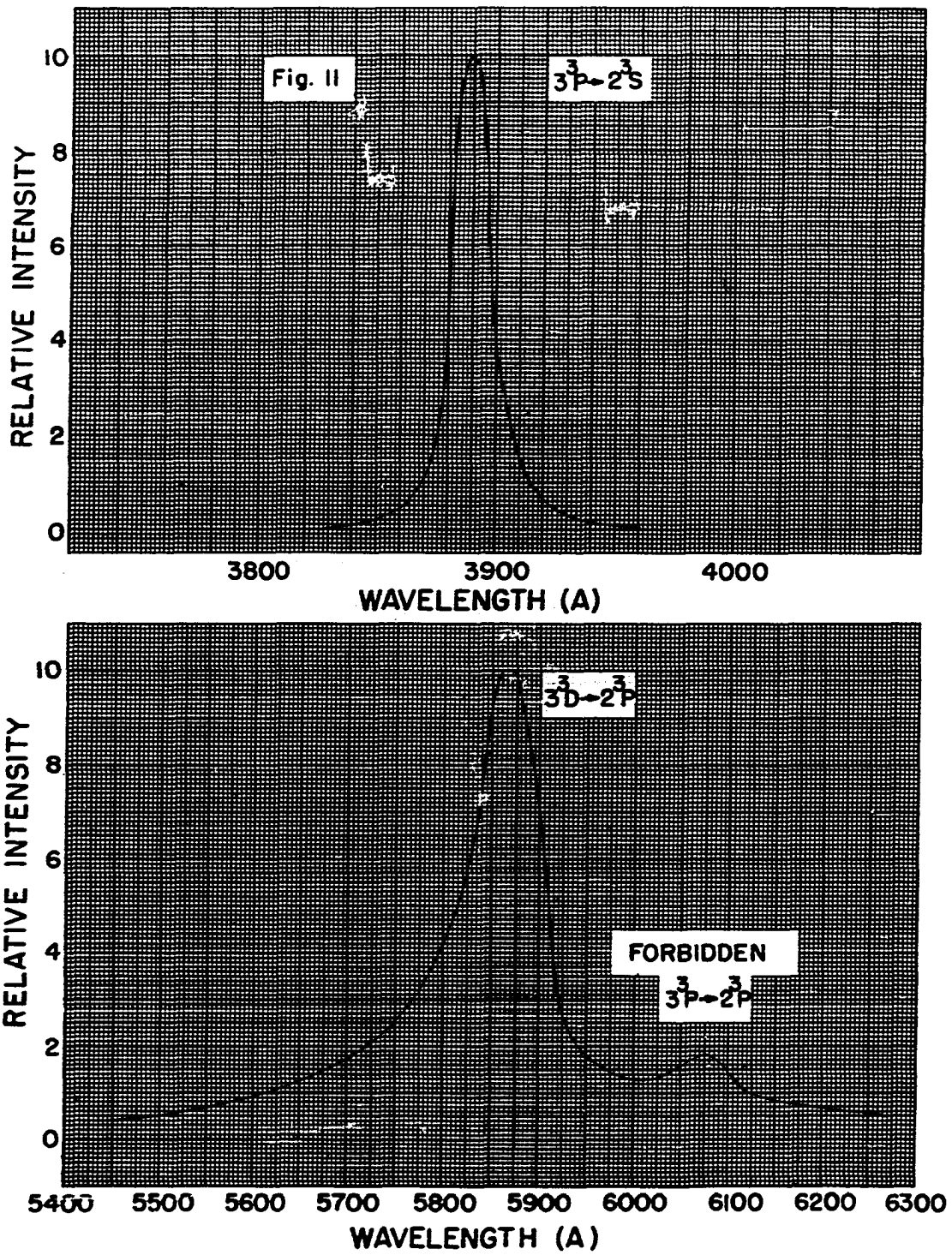

Fig. 11. Line Shapes from Fig. 10

In order to obtain ratios of intensities of forbidden lines to allowed lines, and continuum to allowed lines, it was necessary to assume shapes for the base and for one of the lines. The term "base" as used here means the spectrum in the region of a line which is not due to the line itself, i.e., continuum plus other lines. The base intensity profile was assumed to follow a straight line between the two minima bounding the line or pair of lines. Shapes for the allowed lines were estimated and then subtracted from the observed profiles in order to obtain intensities for the forbidden lines. This is treated in Chapter VI.

The width of a line at half maximum intensity was obtained by graphically subtracting the assumed base intensity from the total profile, and if necessary, replotting the difference. As shown in Fig. 11, width measurements on the 5876 A line are essentially indepentent of the contour of the forbidden line. The forbidden line near the 4471 A line is, however, close enough to contribute significantly to the measured width, so no measurements of half-widths were attempted. The peak intensities of the permitted and forbidden lines were compared, however, and line shifts were measured for the allowed 4471 A transition and the forbidden 4470 A transition.

Broadening and shift data taken from time-integrated spectra are presented in Table I. The absence of values for certain lines at certain pressures implies that the lines were not visible on the spectrogram due to low intensities at low pressures or that they were broadened to such an extent that no effort was made to locate centers or measure widths.

Initial pressures of 8, 20, and 35 mm Hg were used because pressures in this range resulted in reflected shocks with temperatures and

TABLE I

DATA FROM TIME-INTEGRATED SPECTRA

Initial Pressure (mm Hg)	Final Temperature (ev)	Electron and Ion Density (10^{17} cm^{-3})	Shift (A)						Width at Half Intensity (A)	
		Line at (A)	3889	4470*	4471	4713	5015	6069*	3889	5876
8	1.74±0.03	2.70±0.35	3±1	14±3	13±3	16±2			10±1	38±4
20	1.82±0.02	5.8 ±0.5	3±1	18±2	15±2	30±2	6±1	8±2	20±2	100±10
35	1.87±0.02	9.3 ±1.2	4±1	29±4	22±4	32±5	13±2	13±2	25±3	187±19

*Forbidden Transition

electron densities of the appropriate order of magnitude to provide a check for certain theories of line broadening and shift. For initial pressures appreciably greater that 50 mm Hg, all lines were so broad and smeared into the continuum as to be useless for quantitative measurements. Initial pressures below 5 mm Hg, for example 2 mm Hg, resulted in a spectrum filled with impurity radiations.

Time-resolved Spectra

Initially the purpose of making time-resolved spectra was to check the assumption that the majority of the light recorded on time-integrated spectra was emitted from helium at kinetic equilibrium behind the reflected shock wave. The spectra in Fig. 8 showed the assumption to be qualitatively valid, but for a more precise evaluation several of the plates were densitometered at three levels in what appeared to be an equilibrium region. No changes in broadening or shift were detected, implying either a negligible change in electron and ion density or a balance between losses by recombination and a long-term relaxation phenomenon leading to ionization -- considered unlikely because of the rapidity with which a steady radiation state is reached near the shock front.

In Fig. 8, where time response is about 1/2 μsec, it may be seen that apparant relaxation times are about as given below:

Initial Pressure (mm Hg)	5	20	35
Relaxation Time (μsec)	1	1/2	<1/2

The indication that the relaxation time is dependent on initial pressure is reasonable, but no effort was made to imply kinetic processes or cross

sections from these rough measurements.

Analysis of time-resolved spectra for line shifts, line widths, intensities, etc., was carried out in a manner much like that for time-integrated spectra. The only difference occurred in the choice of positions on the spectrogram from which the microphotometer traces were taken. On time-resolved spectra the "shock" trace was made along what appeared to be the center of the equilibrium region and the "reference" trace and "half and half" trace were combined into one made along the nearest reference spectrum.

Data from time-resolved spectra are given in Table II. These may be compared with the time-integrated data in Table I.

Initial pressures of 5, 20, and 35 mm Hg were chosen for the following reasons: Pressures below 5 mm Hg would not produce sufficient light from the reflected shock wave to be recorded by the apparatus in use. The optimum initial pressure, judging from time-integrated spectra, for observing line broadening and shift seemed to be about 20 mm Hg. A pressure of 35 mm Hg was the highest for which line centers of the strongly shifted lines at 4713 and 5015 A could be located.

Some numbers which are proportional to the ratio of total line intensity to continuum intensity at the line are given in Table III. These numbers were computed by dividing the area under the line shape (relative intensity vs. wavelength) by the relative intensity of the continuum in the vicinity of the line. These data will be considered later in connection with self-absorption. Of particular interest is the fact that the ratio for the 5876 A line does not vary in the same way with initial shock tube pressure as does that for the 3889 A line.

TABLE II

DATA FROM TIME-RESOLVED SPECTRA

Initial Pressure (mm Hg)	Final Temperature (ev)	Electron and Ion Density (10^{17} cm^{-3})	Shift (A)						Width at Half Intensity (A)	
		Line at (A)	3889	4470*	4471	4713	5015	6069*	3889	5876
5	1.70±0.03	2.2±0.3	2±1	14±2	12±2	9±2		6±2	12±2	42±10
20	1.82±0.02	5.8±0.5	4±1	20±2	19±2	26±3	7±2	9±2	18±2	144±30
35	1.87±0.02	9.3±0.8	7±1	25±2	26±2		13±2	11±2	29±2	280±30

*Forbidden Transition

TABLE III

LINE VS. CONTINUUM INTENSITY*

Initial Pressure (mm Hg)	Line at 3889 A	Line at 5876 A
20	1	1
35	0.76	0.71

*Numbers in the table are proportional to the ratio of the total intensity of the line to the intensity of the continuum in the vicinity of the line.

Smear Camera Photographs

The state of the gas behind the reflected shock wave could be calculated from initial conditions and the shock velocity in the primary wave. These calculations and attendant assumptions are discussed in the next chapter. Because the shock hydrodynamic equations for a plane (one-dimensional) shock wave were used, only the spectra from shots where a plane wave was observed were analyzed quantitatively. Methods for measuring the velocity of the primary shock wave were discussed in Chapter III. Measurements of the slope of the shock line lacked precision because the shock line was not luminous and its position had to be implied from its endpoints. This procedure required the assumption that changes of velocity over the length of the tube were negligible.

More precise measurements of shock velocity employed shock tube transit times. Errors in the measurements of tube lengths, s, and transit times, t, were no greater than 2 mm and 0.1 μsec, respectively. On this

basis the estimated maximum error in measurement of the shock velocity for any individual shot might be expected to be

$$dV = \sqrt{\left(\frac{\partial V}{\partial s}\,ds\right)^2 + \left(\frac{\partial V}{\partial t}\,dt\right)^2} = \sqrt{\left(\frac{ds}{t}\right)^2 + \left(\frac{sdt}{t^2}\right)^2}$$

and for the worst set of length and transit time measurements, this amounted to 0.12 mm/μsec for a tube 10" long and 0.04 mm/μsec for a tube 30" long, where V = 12.47 mm/μsec, or 1% for a 10" tube and 0.3% for a 30" tube.

Data from transit time measurements are plotted on Fig. 12 to show reproducibility from shot to shot. Two tube lengths, 10" and 30", were used to detect any measurable attenuation of the shock wave within a 30" run. Figure 12 suggests that the average velocity over the first 10" of tube length may be less than that for the full run of 30". This may indeed be the case because of the time required to accelerate the Furane surface by explosive gases, but the difference is so slight as not to be definitely established with the technique used here. Also there is no known reason why the velocity for 20 mm Hg initial pressure should be higher than that for 5 mm Hg initial pressure as is indicated in Fig. 12. Since these trends were within the experimental reproducibility, they were attributed to random differences in shock tubes, and the data from 30" tubes were averaged to provide a single velocity for all pressures. This is reasonable if it is recalled that explosive gases under a pressure of several hundred thousand atmospheres are expanding into a region with a pressure of less than 0.1 atm, and thus small changes in initial shock tube pressure would not be expected to cause a measurable change in shock velocity.

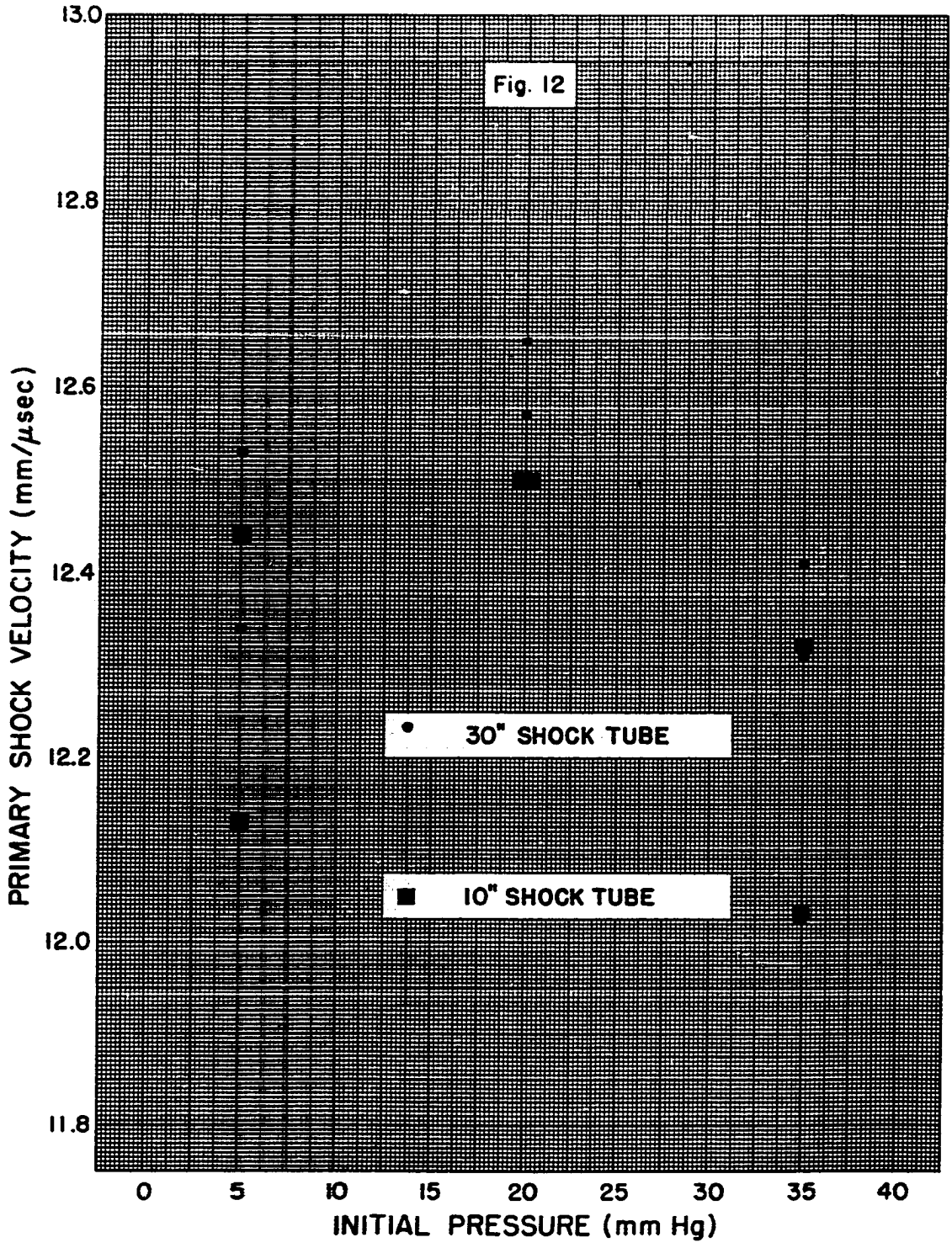

Fig. 12. Shock Velocity Measurements from Transit Times

The mean primary shock velocity for the six 30" tubes was 12.47 mm/μsec, with a standard deviation, S_o, of 0.13 mm/μsec for the six measurements. Thus it is seen that the estimated upper limit for the measurement error, 0.04 mm/μsec, introduced a negligible uncertainty into S_o.

In order to predict an uncertainty for the average shock velocity of a set of additional shots in which the spectral results were to be averaged, it was necessary to calculate the way in which the mean of n additional measurements, M_n, would deviate from the mean, $M_o = 12.47$, of the $n_o = 6$ measurements. Using a result from Ostle[2] for estimating confidence intervals for the difference of two population means, we assume all measurements to be taken from a single normal distribution. The difference of means, d, of pairs of sets of measures will be normally distributed about zero with a standard deviation,

$$S_d = \sqrt{\frac{S_o^2}{n_o} + \frac{S^2}{n}}$$

In this case, however, it was assumed that $S = S_o$ since no value for S would ever be obtained. This gives

$$S_d = S_o\sqrt{\frac{1}{n_o} + \frac{1}{n}}$$

The quantity

$$t = \frac{d}{S_d} = \frac{M_o - M_n}{S_o\sqrt{\frac{1}{n_o} + \frac{1}{n}}}$$

is a Student's t distribution with n_o+n-2 degrees of freedom, but since S_o was always based on only six measurements, only $n_o-1 = 5$ degrees of freedom were available. By this approximate method we have that the

---

[2] B. Ostle, Statistics in Research (Iowa State College Press, 1954), p. 63.

probability, P, of M_o-M being between

$$\pm S_o \sqrt{\frac{1}{n_o} + \frac{1}{n}} \; t_{e(5)}$$

is 1-e, where $t_{e(5)}$ is obtained from a table of the t distribution with $e = P\{|t| > \text{value in table}\}$ and $n_o - 1 = 5$ is the degrees of freedom in the table. For a 90% confidence interval the result is

$$M_n = M_o \pm (0.13)\sqrt{\frac{1}{6} + \frac{1}{n}} \quad (2.015)$$

This value was used for all calculations of the thermodynamic state of the helium behind the reflected shock wave. If, for example, line shift and broadening measurements for three shots made at a single initial pressure were averaged, then the uncertainty in the temperature and ion density would depend on the factor 1/6+1/n = 1/6+1/3.

In a later chapter where experimental results are compared with theoretical predictions, the confidence interval is not indicated but in most cases it would amount to less than ±15% of the theoretically predicted value of line shift or width.

CHAPTER V

HYDROTHERMODYNAMIC CALCULATIONS

Determination of the state of the emitting gas behind a reflected shock wave from the initial conditions and primary shock velocity required calculations based on certain assumptions and approximations as follows:

(1) It was assumed that the flow phenomena in the shock tube could be described by the equations for a one-dimensional shock wave.

The observed planarity and nearly constant velocity of the shock waves tended to justify this assumption experimentally. Here it is implied that heat conduction, radiative cooling, and viscosity losses had a negligible effect on the flow phenomena.

(2) Thermodynamic equilibrium was assumed to exist in finite regions behind the shock fronts.

The steady radiation state which was observed on the time-resolved spectra was believed to represent a region where all relaxation phenomena had been completed and radiative losses caused negligible changes in the thermodynamic coordinates during the period of observation ($\sim$10 μsec).

(3) Reflection of the shock wave was assumed to occur at a perfectly rigid wall.

No motion of the end plate on the shock tube was observed during the first

20 μsec following reflection.

(4) It was assumed that the helium atoms, helium ions, and electrons formed an ideal gas.

(5) The Saha equation was assumed to give the correct ionization constant even though electronic excitation and "pressure ionization" were neglected.

Here "pressure ionization" refers to the effective lowering of the ionization potential when the density of charged particles is not vanishingly small.

These assumptions will be examined in more detail following a presentation of calculational methods and results.

The theory of the one-dimensional shock wave has been treated by several authors.[1,2,3] In particular, Turner and Resler have considered the shock tube as a means of producing a high temperature gaseous source of radiation, and Turner has reviewed the historical development of the shock tube as a research tool.

A conventional method of describing the flow in a shock tube is the x-t diagram shown in Fig. 13, which is essentially a sketch of a smear camera photograph. The density, pressure, temperature, degree of ionization, and particle velocity in region i are denoted by the symbols ρ_i, P_i, T_i, α_i, and u_i, respectively. U and U_R are the velocities of the

---

[1] R. Courant and K. Friedrichs, Supersonic Flow and Shock Waves (Interscience Publishers, Inc., New York, 1948), Vol. I.

[2] E. B. Turner, "The Production of Very High Temperatures in the Shock Tube with an Application to the Study of Spectral Line Broadening," AFOSR TN-56-150, ASTIA Document No. AD 86309 (1956).

[3] E. Resler, S. Lin, and A. Kantrowitz, J. Appl. Phys. 23, 1390 (1952).

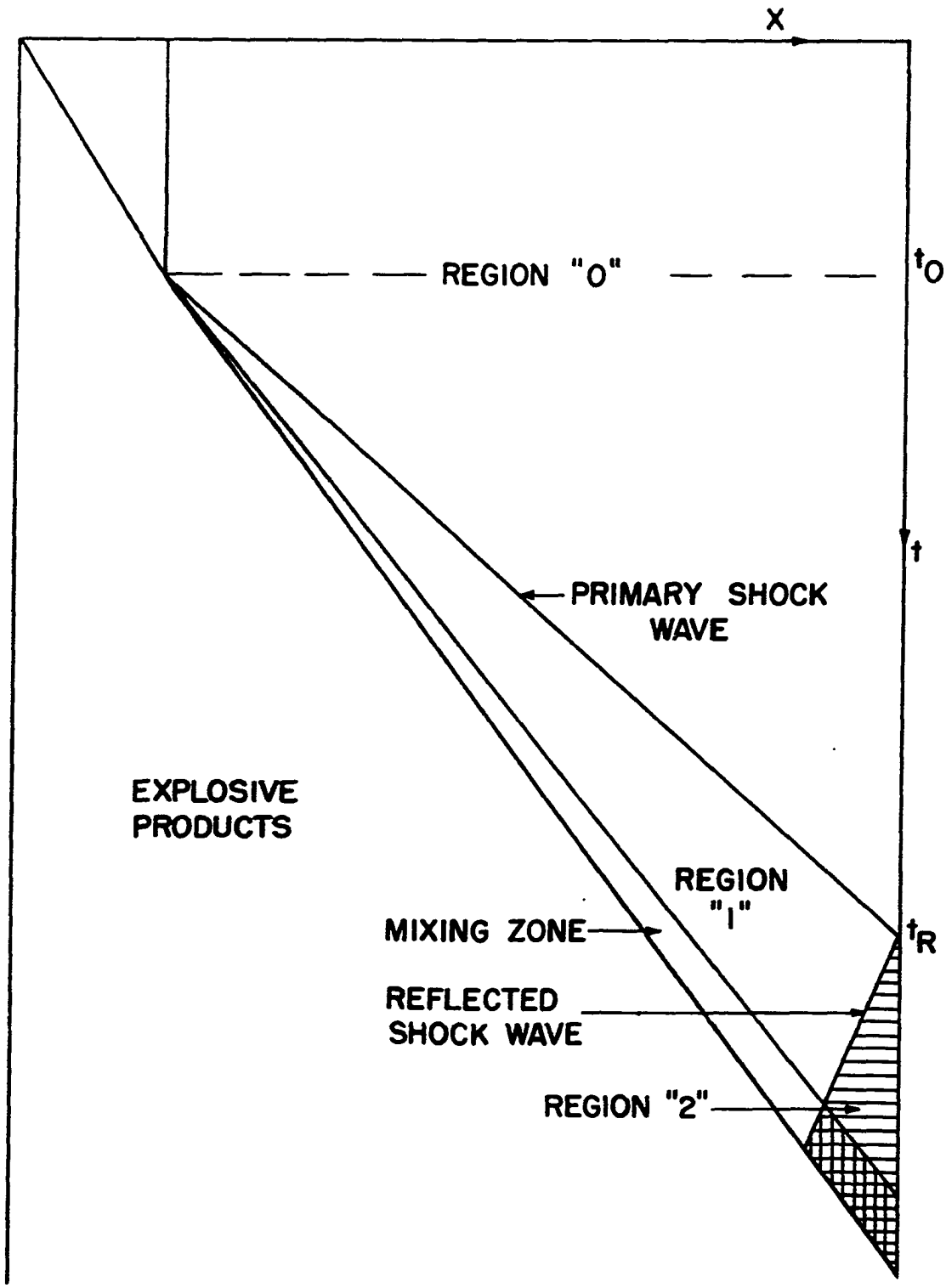

Fig. 13. Distance-Time Diagram of Processes in the Explosive-driven Shock Tube

primary and reflected shock waves respectively. The particle velocities u_0 and u_2 are both zero.

The conservation equations which define a shock wave moving into a material at rest are

$$\rho_1(u_1-U) = -\rho_0 U \qquad \text{(Mass)} \qquad \text{(V-1)}$$

$$\rho_1(u_1-U)^2-\rho_0 U^2 = P_0-P_1 \qquad \text{(Momentum)} \qquad \text{(V-2)}$$

$$\frac{U^2}{2}+H_0 = \frac{(u_1-U)^2}{2}+H_1 \qquad \text{(Energy)} \qquad \text{(V-3)}$$

and the corresponding equations for a reflected shock wave are

$$\rho_1(u_1-U_R) = \rho_2 U_R \qquad \text{(Mass)} \qquad \text{(V-4)}$$

$$\rho_1(u_1+U_R)^2-\rho_2 U_R^2 = P_2-P_1 \qquad \text{(Momentum)} \qquad \text{(V-5)}$$

$$\frac{U_R^2}{2}+H_2 = \frac{(u_1+U_R)^2}{2}+H_1 \qquad \text{(Energy)} \qquad \text{(V-6)}$$

where H_i is the enthalpy per gram of material in region i as shown in Fig. 13. It was assumed that for helium gas

$$P_i = \frac{\rho_i RT_i}{M}(1+\alpha_i) \qquad \text{(V-7)}$$

which leads to

$$H_i = \frac{5}{2}(1+\alpha_i)\frac{RT_i}{M}+\alpha_i\frac{RT_{ion}}{M} \qquad \text{(V-8)}$$

where R is the universal gas constant, M is the molecular weight, and

T_{ion} is the ionization potential in ev multiplied by 11,600°K/ev. The degree of ionization, α_i, can be written as a function of P_i and T_i in the Saha equation

$$\frac{\alpha_i^2}{(1-\alpha_i^2)} P_i = \frac{(2\pi m)^{3/2}(kT_i)^{3/2}(p.f.)_e(p.f.)_{He^+}}{h^3(p.f.)_{He}} e^{-(T_{ion}/T_i)} \quad (V\text{-}9)$$

where the previously undefined quantities are

h = Planck's constant

m = reduced mass (essentially the mass of the electron)

k = Boltzmann's constant

$(p.f.)_e = 2$ = internal partition function of the electron

$(p.f.)_{He^+} = 2$ = internal partition function of the helium ion

$(p.f.)_{He} = 1$ = internal partition function of the helium atom

Given the initial state, subscript 0, of the gas and the primary shock velocity, the Eqs. (V-1) through (V-9) define the states of the gas in regions 1 and 2 (see Fig. 13). Eqs. (V-1), (V-2), and (V-3) can be solved independently of (V-4), (V-5), and (V-6) but the solution of each system requires numerical iteration methods because of the trancendental nature of the Saha equation.

R. E. Duff, of LASL, provided the author with complete solutions for initial pressures ranging from 2 to 200 mm Hg at an initial temperature of 300°K and primary shock velocities ranging from 6 to 14 mm/μsec. Duff had previously coded a general problem in which the shock equations were solved for complicated systems of reacting gases on an IBM 701 Data Processing Machine. It was necessary to provide the machine with P_0, T_0, T_1, and the standard Gibbs free energies, $G^\circ = H^\circ - TS^\circ$, at a pressure

of 1 atm as a function of temperature for the reactants and products. The machine solved the equation

$$\ln K = -\frac{\Delta G^\circ}{RT} \qquad \text{(V-10)}$$

simultaneously with the shock equations for both the primary and reflected shock waves. Equation 10, where $K = \alpha^2/(1-\alpha^2)$, is equivalent to the Saha equation.

Results of these calculations are presented in graphical form in Figs. 14 through 19. Conditions in region 2 (behind the reflected shock wave) are plotted as a function of U.

As shown in Chapter IV, the mean value of U predicted for a set of n shots for which spectral characteristics were to be averaged was 12.47 mm/μsec with a 90% confidence interval of $\pm 0.26\sqrt{1/6 + 1/n}$ mm/μsec. Corresponding intervals for the temperature, T_2, and electron density, n_e, have been plotted as a function of initial pressure, P_0, in Fig. 20 for two values of n. These curves show graphically the effect of variations in U on T_2 and n_e. Fig. 20 will be applied later in comparing experimental results with theoretical predictions of spectral characteristics.

At this point some of the assumptions enumerated at the beginning of this chapter can be examined in more detail. The assumption of a perfect reflection was checked by comparing the measured reflected shock velocity with that calculated from the measured primary shock velocity and initial conditions. This agreement was easily within experimental error. Further, the expansion due to the motion of the reflecting wall can be estimated by using calculated pressures, P_2. The maximum force

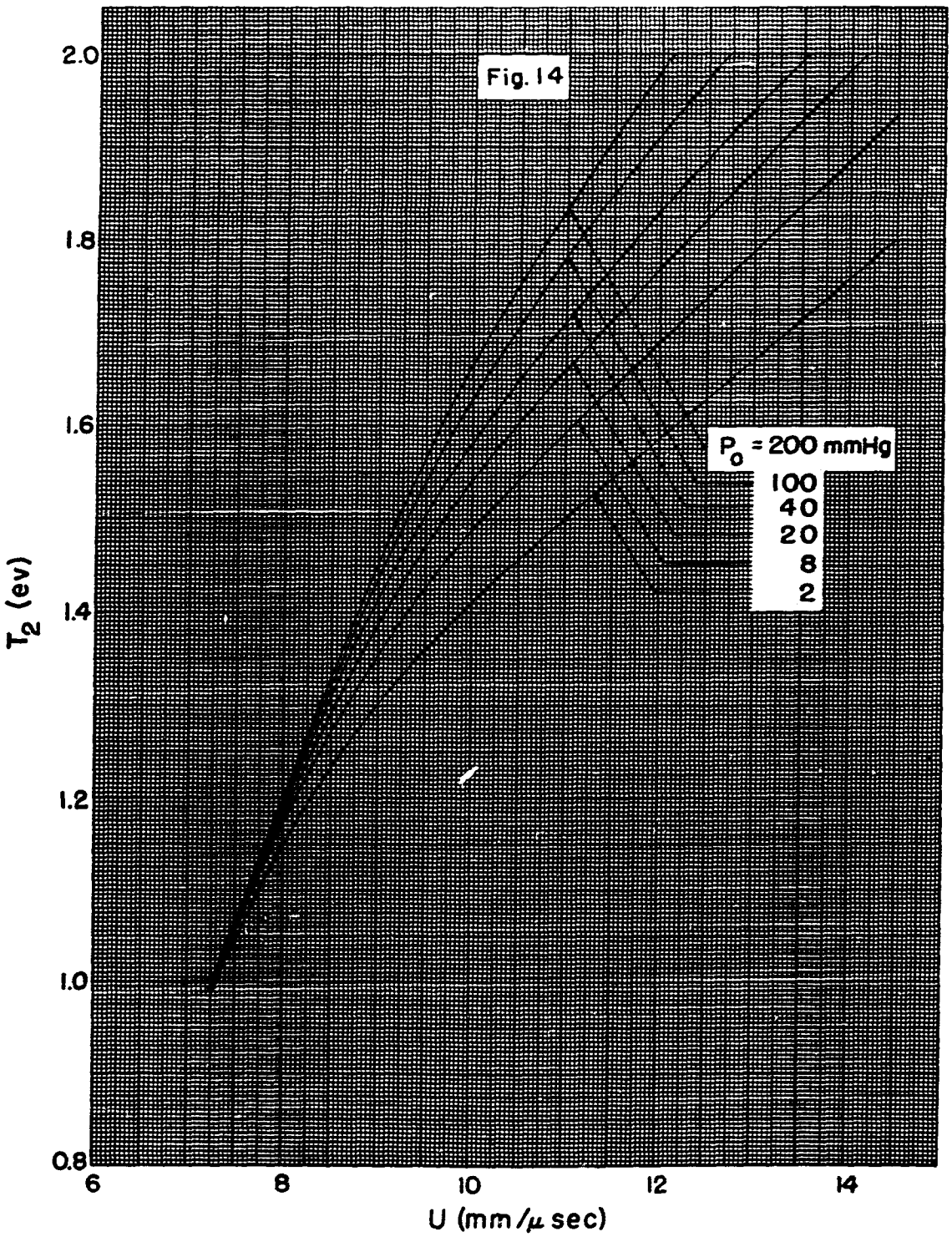

Fig. 14. Temperature behind the Reflected Shock Wave

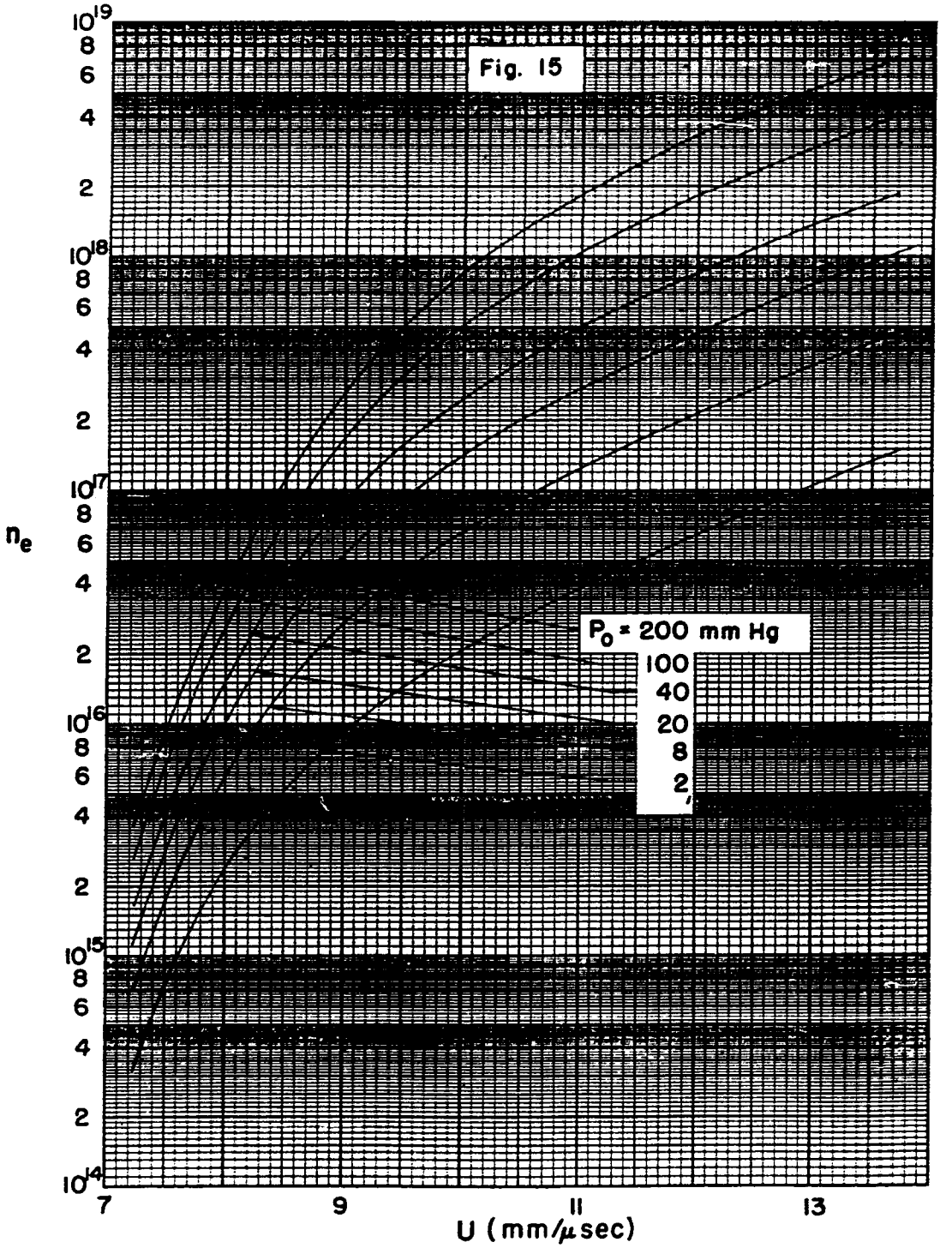

Fig. 15. Electron and Ion Density behind the Reflected Shock Wave

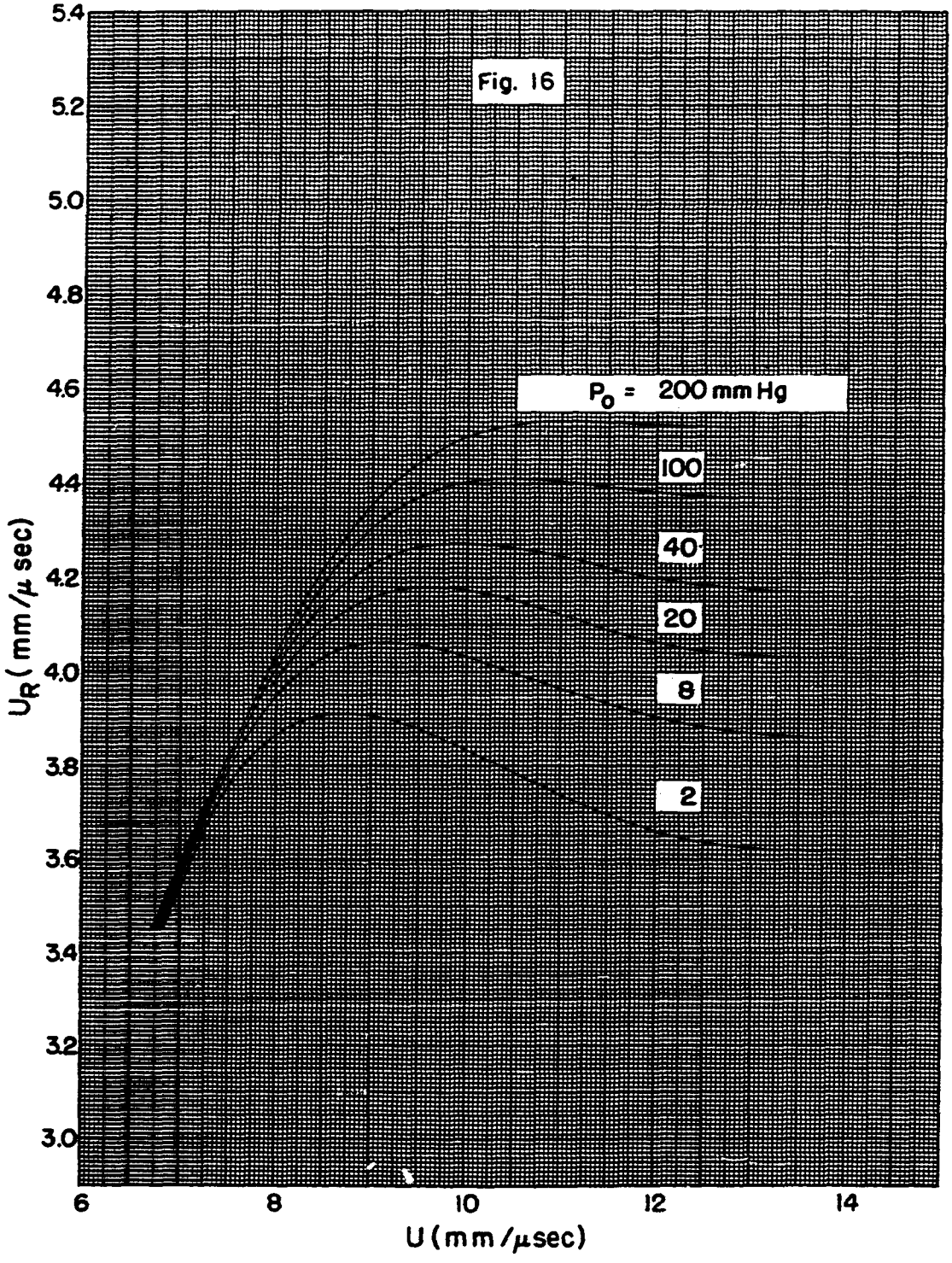

Fig. 16. Velocity of the Reflected Shock Wave

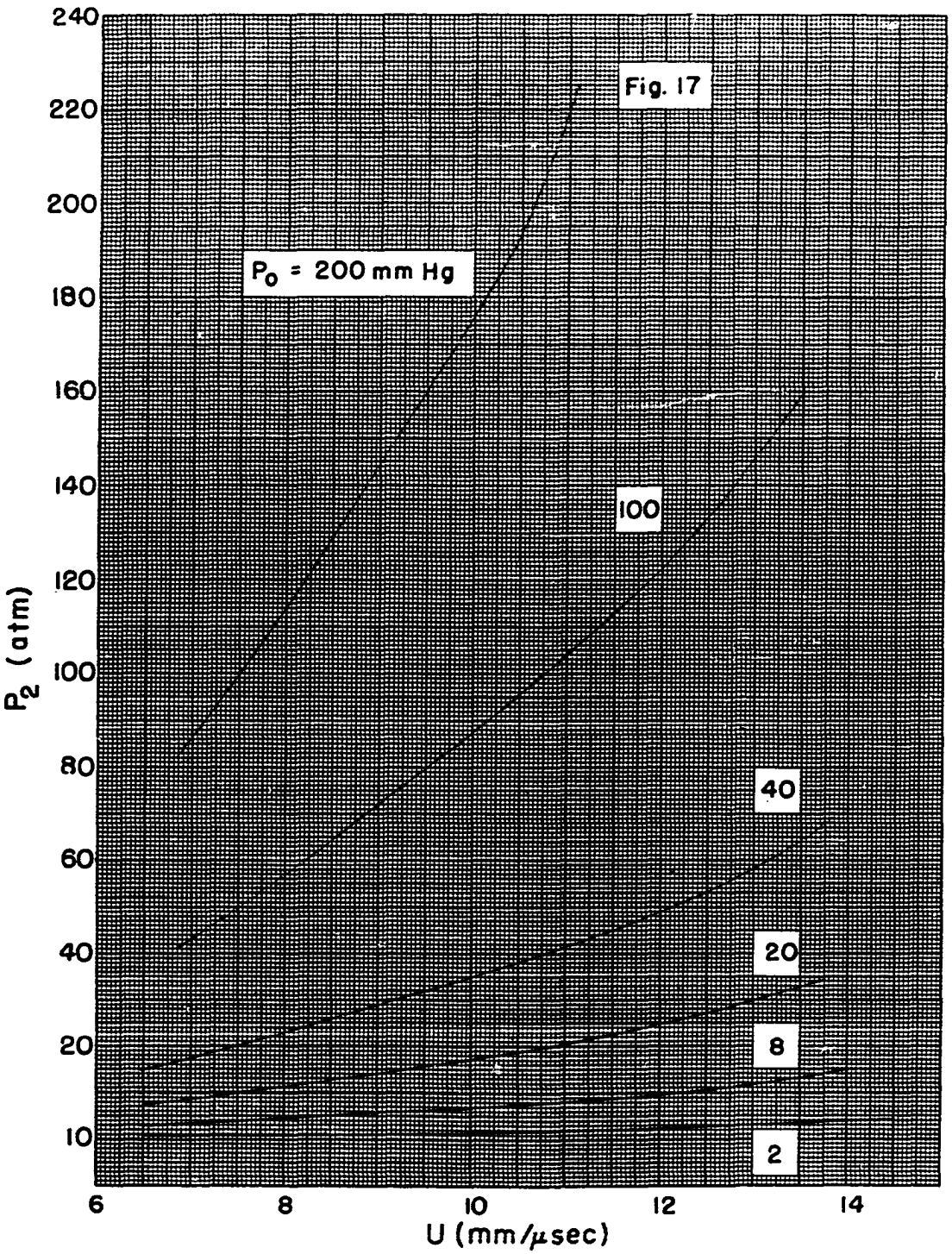

Fig. 17. Pressure behind the Reflected Shock Wave

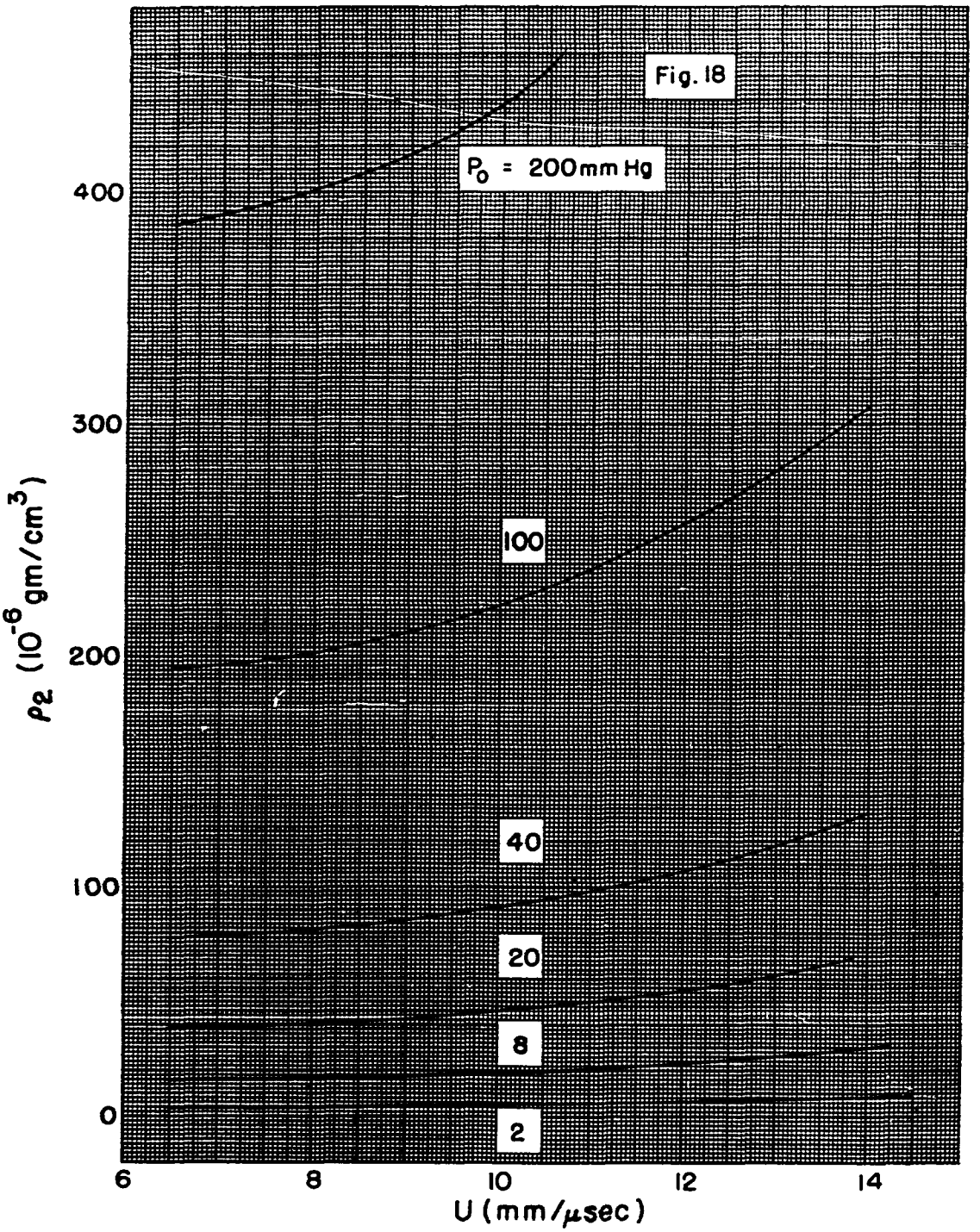

Fig. 18. Density behind the Reflected Shock Wave

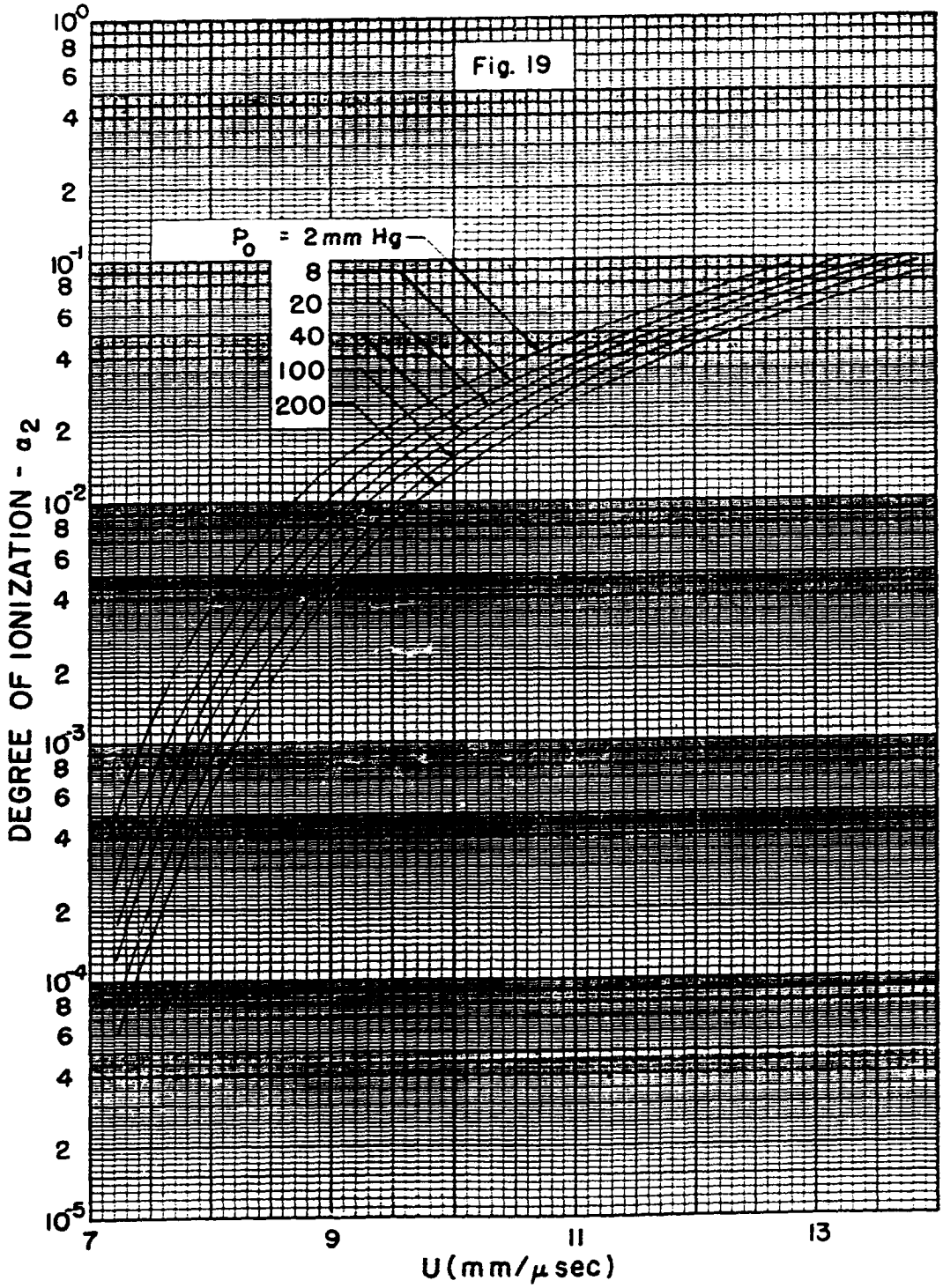

Fig. 19. Degree of Ionization behind the Reflected Shock Wave

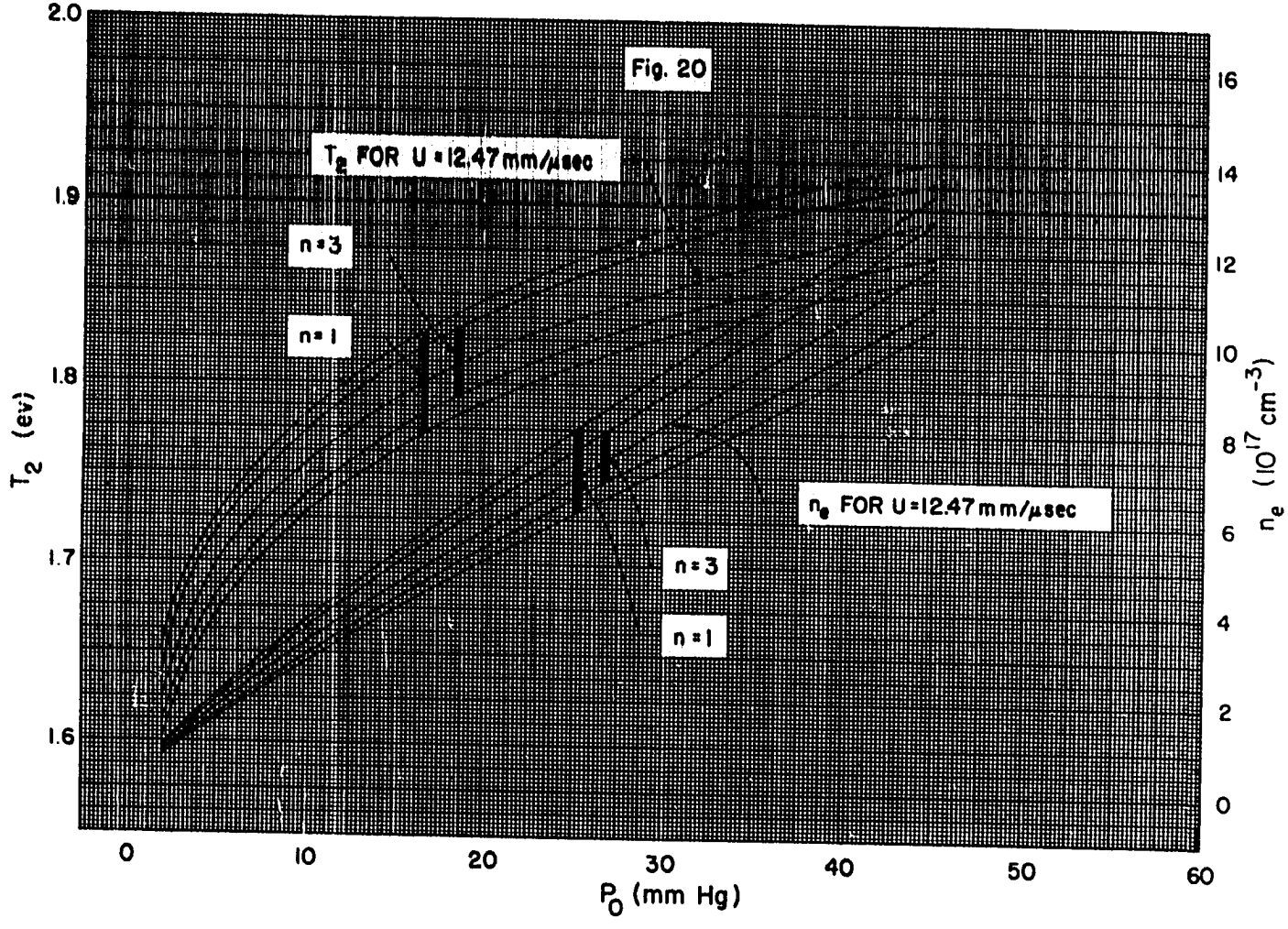

Fig. 20. Ninety Per Cent Confidence Intervals for n = 1 and n = 3

per unit area, corresponding to an initial pressure of 40 mm Hg, was about 50 atm, and the mass per square centimeter of the reflecting wall, ρ_g, was about 1.6 grams. Then the distance d, moved by the end plate during the lifetime of the reflected shock wave (~10 μsec) was

$$d = \frac{1}{2}\frac{P_2}{\rho_g} t^2 \simeq 1.6 \times 10^{-5} \text{ cm}$$

This would correspond to a fractional error in ρ_2 of about $1.6 \times 10^{-5}/4 = 4 \times 10^{-6}$ which is certainly negligible.

The assumption that radiation losses were negligible in the region behind the reflected shock wave can be substantiated somewhat by rough calculations based on data on Fig. 20. The total enthalpy per cubic centimeter, H_v, of the gas in region 2, again for an initial pressure of 40 mm Hg, was

$$H_v = \frac{5}{2} N(1+\alpha_2)kT_2 + \alpha_2 NkT_{ion}$$

where N = nuclei/cm^3 = 1.7×10^{19}

$\alpha_2 = 0.06$

$T_2 = 22{,}000°K$

$H_v = 1.8 \times 10^8$ ergs/cm^3

Losses due to bremsstrahlung, recombination, and line radiation will be discussed separately and each will be compared with H_v.

According to Spitzer[4] the energy radiated in the form of bremsstrahlung from a partially ionized gas is

---

[4] L. Spitzer, Jr., Physics of Fully Ionized Gases ("Interscience Tracts on Physics and Astronomy," Vol. 3; Interscience Publishers, Inc., New York, 1956).

$$E_b = 1.435 \times 10^{-27}\, z^2 T^{1/2}\, g\, N_e^2 \text{ erg/cm}^3\ \mu\text{sec}$$

where $z = 1$ and $g \simeq 1$. For the gas in region 2 with T_2, N, and α_2 as given above

$$E_b = 2.5 \times 10^5 \text{ erg/cm}^3\ \mu\text{sec}$$

This amounts to about 0.14% of the enthalpy per microsecond.

Recombination radiation may be divided into two limiting cases; that which is blockaded and thus causes energy loss only near the surface of the source, and that radiation to which the gas is essentially transparent. When radiative recombination to the ground state occurs with electrons having a most probable kinetic energy of 1.9 ev, the radiation will have a wavelength of about 470 A. According to Huang,[5] the atomic photo-ionization absorption coefficient, a, is about 5×10^{-18} cm^2. Then the distance required to re-absorb 90% of this radiation is

$$x_{0.01} = \frac{\ln 0.01}{-N(1-\alpha)a} \ll 0.6 \text{ mm}$$

Thus recombination to the ground state will not contribute appreciably to radiative losses. Consider now recombination radiation to which the gas is essentially transparent. The total rate of recombination to excited states for helium as given by Allen[6] for a temperature of 22,000°K is

$$\frac{dn_e}{dt} \simeq 2.3 \times 10^{14}\, n_e^2$$

---

[5] S. S. Huang, Astrophys. J. 108, 354 (1948).

[6] C. W. Allen, Astrophysical Quantities (University of London, The Athlone Press, 1955), p. 91.

If the average energy of the emitted photons is about 4 ev, the energy loss by radiative recombination per microsecond is about

$$E_r \simeq 1.5 \times 10^5 \text{ erg/cm}^3 \ \mu\text{sec}$$

This is less than 0.1% of the calculated enthalpy per cubic centimeter. Thus even though the rate of recombination was apparently very large, the energy loss was negligible. This implies that processes were constantly contributing to ionization in an effort to maintain an equilibrium distribution consistent with the energy density.

Energy losses by line radiation can be treated by using Einstein "A" coefficients as tabulated by Allen.[7] An "average" atomic absorption coefficient for a line is, according to Aller,[8]

$$\overline{a_\nu} = \frac{B_{n'n} h\nu}{4\pi \overline{\Delta\nu}}$$

where $\overline{\Delta\nu}$ is an "effective width" of the line and

$$B_{n'n} = \frac{A_{n'n}}{2h\nu^3} \frac{g_n}{g_{n'}} c^2$$

with g_n denoting the multiplicity of level n. Thus

$$\overline{a_\nu} = \frac{A_{nn'} \lambda^2}{8\pi \overline{\Delta\nu}} \frac{g_n}{g_{n'}}$$

The "average" linear absorption coefficient is then

---

[7] Ibid., p. 68.

[8] L. H. Aller, Astrophysics (The Roland Press Company, New York, 1953), p. 131.

$$\overline{k_\nu} = \overline{a_\nu} N_{n'} = \frac{N_{n'} A_{nn'} \lambda^2}{8\pi\Delta\nu} \frac{g_n}{g_{n'}}$$

where $N_{n'}$ is the density of particles in level n'. If this formula is applied to a resonance line, say $\lambda = 584$ A, by using the same values as before for T_2 and n_e, it is shown that resonance radiation is self-absorbed sufficiently so that any energy loss is negligible. For the line at $\lambda = 584$ A,

$$N_{n'} = 1.5 \times 10^{19} \text{ cm}^{-3}$$

$$A_{nn'} = 2.33 \times 10^{9} \text{ sec}^{-1}$$

$$\frac{g_n}{g_{n'}} = 3$$

$$\overline{\Delta\lambda} < 2 \text{ A}$$

$$\overline{\Delta\nu} = \frac{c}{\lambda^2} \Delta\lambda < 1.7 \times 10^{13} \text{ sec}^{-1}$$

where the value of $\overline{\Delta\lambda}$ results from a rough calculation of ion broadening which is treated in the following chapter. When calculated with the above numbers, $\overline{k_\nu} > 10^3$ cm^{-1} and the thickness for 99% re-absorption is less than 0.05 mm.

The light from strong nonresonance lines is, however, only slightly self-absorbed, and the energy radiated by a typical transition can be calculated roughly by the following formula

$$E_L = \frac{N_{1s^2}\, g_n\, e^{-E_n/kT} A_{nn'} h\nu}{10^6} \text{ erg/cm}^3\ \mu\text{sec}$$

The line at $\lambda = 3889$ A is a typical strong line in the visible region of the spectrum, and the numbers to be used in the equation for E_L are

$N_{1s^2} \simeq 1.5 \times 10^{19}$ cm^{-3} = ground state atoms per cubic centimeter

$g_n = 5$

$E_n = 36.75 \times 10^{-12}$ erg

$A_{nn'} = 9.4 \times 10^{6}$ sec^{-1}

$h\nu = 5.1 \times 10^{-12}$ erg

and the energy radiated is about 2.8×10^{4} ergs/cm^3 μsec. This is less than 0.02% of the enthalpy. There is perhaps the equivalent of ten lines which would radiate comparable emounts of energy to that from $\lambda = 3889$ A, so it is estimated that the loss per microsecond by line radiation was about 0.2% of the enthalpy.

In summary, it appears that transitions which terminate in the ground state produced radiation which was blockaded or "imprisoned," and that the sum of bremsstrahlung, recombination, and line radiations could have caused an energy loss of about 7×10^{5} erg/cm^3 μsec. With an initial enthalpy of 1.8×10^{8} erg/cm^3, this would imply a reduction of about 4% in a period of 10 μsec, which is about the lifetime of the reflected shock wave. The above estimates are intended to represent the worst case and serve further to justify the assumption that equilibrium existed behind the reflected shock wave.

The ideal gas assumption can be examined from the standpoint of the Debye-Hückel theory for dilute electrolytes.[9] The electrical Helmholtz free energy per cubic centimeter for a single electrolyte is given by

---

[9] R. Fowler and E. A. Guggenheim, Statistical Thermodynamics (Cambridge University Press, London, 1949).

$$F_v^{el} = -\frac{2}{3}\pi^{1/2} NkT \left[\frac{\pi^{1/3} z^2 e^2}{V^{-1/3} DkT}\right]^{3/2} \qquad \text{(V-11)}$$

where $F_v^{el} = E_v^{el} - TS_v^{el}$ (subscript v indicates "per unit volume")

$D = 1$ = dielectric constant of neutral helium gas

$N = 2n_e$ = sum of electrons and ions per unit volume

k = Boltzmann's constant

e = electronic charge

$z = 1$ = numerical charge of the ion

T = absolute temperature

$V = 1$ = volume

F_v^{el} is approximately the change in Helmholtz free energy that would take place if the ions and electrons in a partially ionized gas were discharged at constant volume and constant N. Substitution of the numerical values of n_e and T for region 2, corresponding to an initial pressure of 40 mm Hg in the shock tube yields

$$F_v^{el} = 2 \times 10^5 \text{ ergs/cm}^3$$

The electrical enthalpy $H^{el} = E^{el} + P^{el}V$ is obtained from the thermodynamic relations

$$P = -\left(\frac{\partial F}{\partial V}\right)_{N,T} \qquad \text{and} \qquad S = -\left(\frac{\partial F}{\partial T}\right)_{N,V}$$

which lead to

$$H_v^{el} = 2F_v^{el} = -4 \times 10^5 \text{ ergs/cm}^3$$

Thus the ideal gas assumption caused perhaps a 0.2% error in the calculated enthalpy.

The validity of the two approximations employed in the Saha

equation can be discussed in terms of the Debye-Hückel results which appear in the previous paragraph. The effect of "pressure ionization," i.e., apparent lowering of the ionization potential from that of an ideal gas, can be estimated in the following manner where the electrical effects are included in the ionization equilibrium relation.

The condition for equilibrium is

$$\sum \mu_i \nu_i = 0 \qquad \text{(V-12)}$$

where μ_i = partial potential of species i

ν_i = stoichiometric coefficient of species i

If Guggenheim[10] is followed in the evaluation of μ_i,

$$\mu_i = \mu_i^o + kT \ln x_i + kT \ln \frac{P}{P^o} + \mu_i^{el} \qquad \text{(V-13)}$$

where μ_i = partial potential per particle of species i

μ_i^o = partial potential per particle of pure species i at $P = P^o$

k = Boltzmann's constant

T = absolute temperature

x_i = mole fraction of species i

P = pressure

P^o = standard pressure

μ_i^{el} = nonideality term

Usually, for neutral gases, the term corresponding to μ_i^{el} is a function of second virial coefficients; however, for present purposes μ_i^{el} will not be evaluated for individual species. Substituting Eq. (V-13) into (V-12) gives

---

[10] E. A. Guggenheim, Thermodynamics (Interscience Publishing Company, New York, 1950), p. 93.

$$\sum \mu_i^{\circ} \nu_i + kT \ln \prod x_i^{\nu_i} + kT \ln \prod \frac{P^{\nu_i}}{P^{\circ}} + \sum \mu_i^{el} \nu_i = 0$$

If $P^{\circ} = 1$ this becomes

$$-kT \ln P^{\Delta\nu} \prod x_i^{\nu_i} = \sum \mu_i^{\circ} \nu_i + \sum \mu_i^{el} \nu_i$$

or,

$$P^{\Delta\nu} \prod x_i^{\nu_i} = \exp\left(-\sum \mu_i^{\circ} \nu_i/kT\right) \exp\left(-\sum \mu_i^{el} \nu_i/kT\right) \qquad \text{(V-14)}$$

Equation (V-14) is equivalent to the Saha equation (V-9) for an ideal gas multiplied on the right by a factor

$$\exp\left(-\sum \mu_i^{el} \nu_i/kT\right)$$

which is interpreted as

$$\mu^{el}/kT = \Delta T_{ion}/2T$$

where ΔT_{ion} is a part of the ionization potential due to non-ideality. The factor 1/2 in $\Delta T_{ion}/2T$ accounts for the fact that μ^{el} is the partial electrical potential per charged particle and ΔT_{ion} is the change in ionization potential per pair of charged particles. In order to evaluate μ^{el} recall that

$$\mu = \left(\frac{\partial F}{\partial N}\right)_{T,V}$$

where N is the total number of charged particles as in Eq. (V-11). From Eq. (V-11) for F_v^{el},

$$\mu^{el} = \left(\frac{\partial F_v^{el}}{\partial N}\right)_{T,V} = \frac{3}{2} \frac{F_v^{el}}{N}$$

so that

$$\Delta T_{ion} = \frac{2\mu^{el}}{k} \simeq \frac{3F_v^{el}}{kN} = -2.2 \times 10^3 °K \text{ or } -0.19 \text{ ev}$$

Thus, for the conditions behind the reflected shock wave, the effective

ionization potential might be as much as 0.2 ev lower than that for an ideal gas. The extent to which the calculated ion density would have been increased if interactions had been considered can be estimated in the following manner. For small α, degree of ionization,

$$\alpha \propto e^{-T_{ion}/2T}$$

Inserting the value just obtained for ΔT_{ion} and the value of T_2 in region 2 for the conditions used previously, we obtain

$$\frac{d\alpha}{\alpha} \propto \frac{-\Delta T_{ion}}{2T_2} = 0.05$$

Therefore, a consideration of the nonideality of the emitting gas in region 2 would have tended to increase the calculated ion density by about 5%.

On the other hand, if, instead of assuming the internal partition function of the neutral helium atoms to be 1, it had been calculated more precisely as a function of temperature and effective ionization potential, a tendency to reduce the degree of ionization would have followed.

These efforts to justify the assumptions which were made in the hydrothermodynamic calculations lead to the conclusion that errors due to the assumptions were small compared to experimental uncertainties. For this reason calculated results were used as they appear in Figs. 14 through 20, with no further recognition of their inexactness due to cooling, lowering of the ionization potential, etc.

The experimental spectral data in Tables I and II can be associated with corresponding thermodynamic states through Fig. 20.

CHAPTER VI

COMPARISON WITH THEORY

The following features of the visible spectrum of helium behind a strong shock wave were observed either quantitatively or qualitatively:

(1) All observable lines were broadened, some asymmetrically, and some were shifted a measurable amount. These effects increased with increasing initial gas density.

(2) No lines were observed which originated at levels with principal quantum number, n, greater than 4 -- depression of the series limits.

(3) Lines were observed at wavelengths corresponding to shifted positions of normally forbidden transitions.

(4) Appreciable continuum radiation appeared throughout the visible spectrum.

In the following pages various theories are employed to predict these effects and in some cases their interrelationships.

Since the spectral distribution of light escaping from a finite depth of an emitting volume depends on the depth and absorption coefficient it is also necessary to discuss radiation transfer to some extent.

Line Broadening and Shift

One of the primary motivations for the work described in this

thesis was supplied by Bennett Kivel[1] in a theory concerned with the effects of electrons on line shape and position in partially ionized helium gas. Kivel predicts that the effects of the fast electrons will be comparable to the effects of the relatively slow helium ions at a temperature of the order of 1 ev and ion and electron densities of 10^{17} cm^{-3} or greater.

The broadening and shift of spectral lines stem from many causes; the relative importance of these depends on the conditions within the emitting gas. In the present application the effect of interactions with charged particles was so great that the other sources of broadening and shift were negligible. Among those neglected effects are dipole quadrupole, and van der Waals interactions; radiation damping which provides the "natural" line width; and Doppler broadening.

The interaction of charged particles with a radiating atom has been treated for two limiting cases, that in which the emitting atom is assumed to be in a slowly varying field produced by the surrounding particles, and that in which the emitting atom is disturbed by discrete encounters.

Before applying certain of these theories, criteria for their validity will be discussed briefly. If the field of a charged particle is assumed to be effective in perturbing an atom over a range equal to the mean ionic separation, d, then the time $\tau = d/v$ will approximate the duration of the perturbation. Corresponding to τ there will be an uncertainty in angular frequency, $\Delta\omega$, according to the uncertainty principle, $\tau\Delta\omega \gg 1$. If the energy uncertainty corresponding to $\Delta\omega$ is less than the observed perturbation, then a slowly varying field is evident, i.e., the emitted energy is determined by a quasi-stationary pair of perturbed levels.

---

[1] Bennett Kivel, Phys. Rev. 98, 1055 (1955).

If, on the other hand, $\Delta\omega$ corresponds to an energy much greater than the observed perturbation, this implies that the perturbation is effective for only a small portion of the time during which the atom is emitting, and that an "impact" or "discrete encounter" can be assumed.

In the case of helium at a temperature of about 1.8 ev with electron and ion densities of about 10^{18} cm^{-3}, as found in the experimental work, the electrons and ions were the only sifnificant perturbers. Values for $\Delta\omega_{el}$ and $\Delta\omega_{He^+}$ are about 10^{14} and 10^{12} sec^{-1}, respectively. Typical observed perturbations were of the order of 10 A, or about 10^{13} sec^{-1} in the visible spectrum. Thus it appears that a slowly varying field theory is appropriate for the ions and a discrete encounter theory is appropriate for the electrons.

The prediction of the shape and position of a spectral line requires a method of combining the effects of the ions and electrons. This has been done in the following manner:

(1) The splitting of the line due to a quadratic Stark effect was calculated as a function of the electric field due to ions.

(2) An electron-broadened line shape was assigned to each Stark component.

(3) Each component was integrated over an ion field probability distribution function.

(4) The components were added graphically to give a total line shape.

(5) The total line shape was shifted by an amount depending on the electron density and temperature.

For predicting line shapes and positions to compare with experiment several approximations have been introduced into the above procedure.

In treating the ionic effects two questions arise:

(1) What is the effect of a given electric field?

(2) What is the probability that a given field will exist?

In answer to the first of the questions, Bethe[2] employed hydrogen wave functions and helium energy levels in an expression for the quadratic Stark effect. The energy shift of a Stark component is given as

$$\Delta E_{n,l,m} = e^2 F^2 \left(\frac{z^2_{n,l+1,m}}{E_{n,l} - E_{n,l+1}} + \frac{z^2_{n,l,m}}{E_{n,l} - E_{n,l-1}} \right) \qquad \text{(VI-1)}$$

where the shift of the lower state of the transition is neglected. The notation is as follows:

$\Delta E_{n,l,m}$ = energy shift of state with quantum numbers n, l , and m

e = electronic charge

F = electric field

$E_{n,l}$ = energy of unperturbed level with quantum numbers n and l

$z^2_{n,l,m} = (z_{n,l,m;\ n,l-1,m})^2 = \left| \int \psi^*_{n,l,m}\, r \cos\theta\, \psi_{n,l-1,m}\, d\tau \right|^2$

$\psi_{n,l,m}$ = hydrogen wave function for state with quantum numbers n, l , and m

The matrix elements $z^2_{n,l,m}$ are evaluated in Handbuch der Physik (2d ed., Vol. 24, Part I; Verlag Julius Springer, Berlin, 1933) and helium energy levels may be found in Atomic Energy Levels by Charlotte E. Moore, National Bureau of Standards Circular 467 (1949).

Equation (VI-1) is not valid when $\Delta E_{n,l,m}$ is greater than the zero-field separations of the energy levels $E_{n,l} - E_{n,l+1}$ and $E_{n,l} - E_{n,l-1}$. Foster,[3] in a more complete treatment, shows that $\Delta E_{n,l,m}$ becomes

---

[2] H. Bethe, Handbuch der Physik (2d ed., Vol. 24, Part I; Verlag Julius Springer, Berlin, 1933).

[3] J. S. Foster, Proc. Roy. Soc. (London) A117, 137 (1927).

proportional to the first power of the field, F, as F becomes very large. Foster's results are applied in a later section in connection with energy levels having a principal quantum number of 4 or greater.

An answer to the second question concerning the probability that a certain field will exist is provided by the method of Holtsmark.[4] He derived a probability distribution function for the field due to ions, as a function of the ion density. Various corrections to the Holtsmark theory have been made, the most recent of which is due to Breene.[5] If $\beta = F/F_n$, where F_n is given by $2.61\, e n_e^{2/3}$ for an ion density n_e, the probability function $W(\beta)$ is

$$W(\beta)\, d\beta = \frac{4\beta^2 d\beta}{3\pi}\left(1 - 0.462\,\beta^2 + 0.1227\,\beta^4 - 0.02325\,\beta^6 + \ldots\right) \qquad \text{(VI-2)}$$

for small β, and

$$W(\beta)\, d\beta = \frac{d\beta}{\beta^{5/2}}\, 1.496\left(1 + \frac{2.555}{\beta^{3/2}} + \frac{14.43}{\beta^3} + \frac{0}{\beta^{9/2}} + \ldots\right)$$

for large β.

The most pertinent and recent treatment of the effects of electrons on He I lines is that given by Kivel.[6] His is a quantum mechanical treatment based on usual time-dependent perturbation theory. This theory is a specialized version of a more general treatment of electron broadening.[7] The Hamiltonian includes terms for an unperturbed atom and radiation field, the perturber, an interaction between atom and perturber, an

---

[4] J. Holtsmark, Ann. Physik 58, 577 (1919).

[5] R. G. Breene, Jr., Revs. Modern Phys. 29, 94 (1957).

[6] B. Kivel, Phys. Rev. 98, 1055 (1955).

[7] B. Kivel, S. Bloom, and H. Margenau, Phys. Rev. 98, 495 (1955).

interaction between atom and radiation, but neglects interactions between the radiation and the perturber. With the electrons being treated as plane waves, the equations for the time dependent expansion amplitudes are solved and a line width and shift are obtained. Kivel has called the author's attention to two errors in his treatment of helium. The notation z_{2n} is used for the z component of a dipole matrix element, but this should denote the total dipole matrix element r_{2n} when he discusses electron effects. The other error, of arithmetic nature, appears when he calculates line shifts in angstrom units. The values given are too large by a factor 2π.

The corrected theory for the shift of an energy level (independent of m quantum numbers), say n,l, gives

$$\delta_{n,l} = -\frac{2n_e v_\lambda \sigma_\lambda \pi}{3} \sum_{n,l} \left(\frac{r^{n',l'}_{n,l}}{a} \right)^2 \frac{\omega^{n',l'}_{n,l} - \delta_{n,l}}{\left| \omega^{n',l'}_{n,l} - \delta_{n,l} \right|} \qquad \text{(VI-3)}$$

where the sum over n and l includes all states that can be excited by a free electron with velocity v_λ. The notation is as follows:

$\delta_{n,l}$ = energy shift of level n,l in units of $2\pi\nu$

n_e = electron particle density

v_λ = electron velocity

$\sigma_\lambda = \pi/k_\lambda^2$, where k_λ = electron propagation number

a = first Bohr radius

$\omega^{n',l'}_{n,l}$ = energy difference between levels n,l and n',l' in units of $2\pi\nu$

$$\left(r^{n',l'}_{n,l} \right)^2 = \sum_{m'} \left| r^{n',l',m'}_{n,l,m} \right|^2 = \frac{1}{2l+1} \left| R^{n',l'}_{n,l} \right|^2$$

Values for $\left| R^{n',l'}_{n,l} \right|^2$ are tabulated in Handbuch der Physik, (2d ed., Vol.

24, Part I: Verlag Julius Springer, Berlin, 1933). Algebraic subtraction of the shifts of the upper and lower states of a transition gives the shift of a spectral line due to electrons.

Although the predicted shift is independent of level separation, the broadening is not and thus only nearest neighbor states are considered. Kivel's expression for the half width due to electron broadening is

$$\gamma_{n,l} = \frac{2n_e v_\lambda \sigma_\lambda}{3} \sum_{l=l,l+1} \left(\frac{r_{n,l-1}}{a} \right)^2 2 \ln \left| \frac{4\epsilon_\lambda}{E_{n,l} - E_{n,l-1}} \right| \qquad \text{(VI-4)}$$

where $\gamma_{n,l}$ = half width at half intensity of an emission line originating at state n,l (independent of m, and smearing of lower state is neglected) in units of $2\pi\nu$

ϵ_λ = electron kinetic energy

$E_{n,l}$ = energy of level with quantum numbers n and l

Values for v_λ, σ_λ, and ϵ_λ in Eqs. (VI-3) and (VI-4) are taken to be the most probable values for a temperature T when a Maxwellian distribution is assumed. The effect of this assumption is to include the slow electrons in a calculation for effects of discrete encounters, whereas they should probably be included with the slow ions.

Theoretical predictions for the shapes and positions of two of the lines observed in the experiments have been calculated in the following manner. Equation (VI-1) is used to provide a plot of the positions, ν_o in sec^{-1}, of the Stark components as a function of field strength as shown in Fig. 21. Then the shape of each component is approximated by a symmetrical shape, one side of which is shown in Fig. 22. The value of γ, the electron half width, for each component is obtained from Eq.

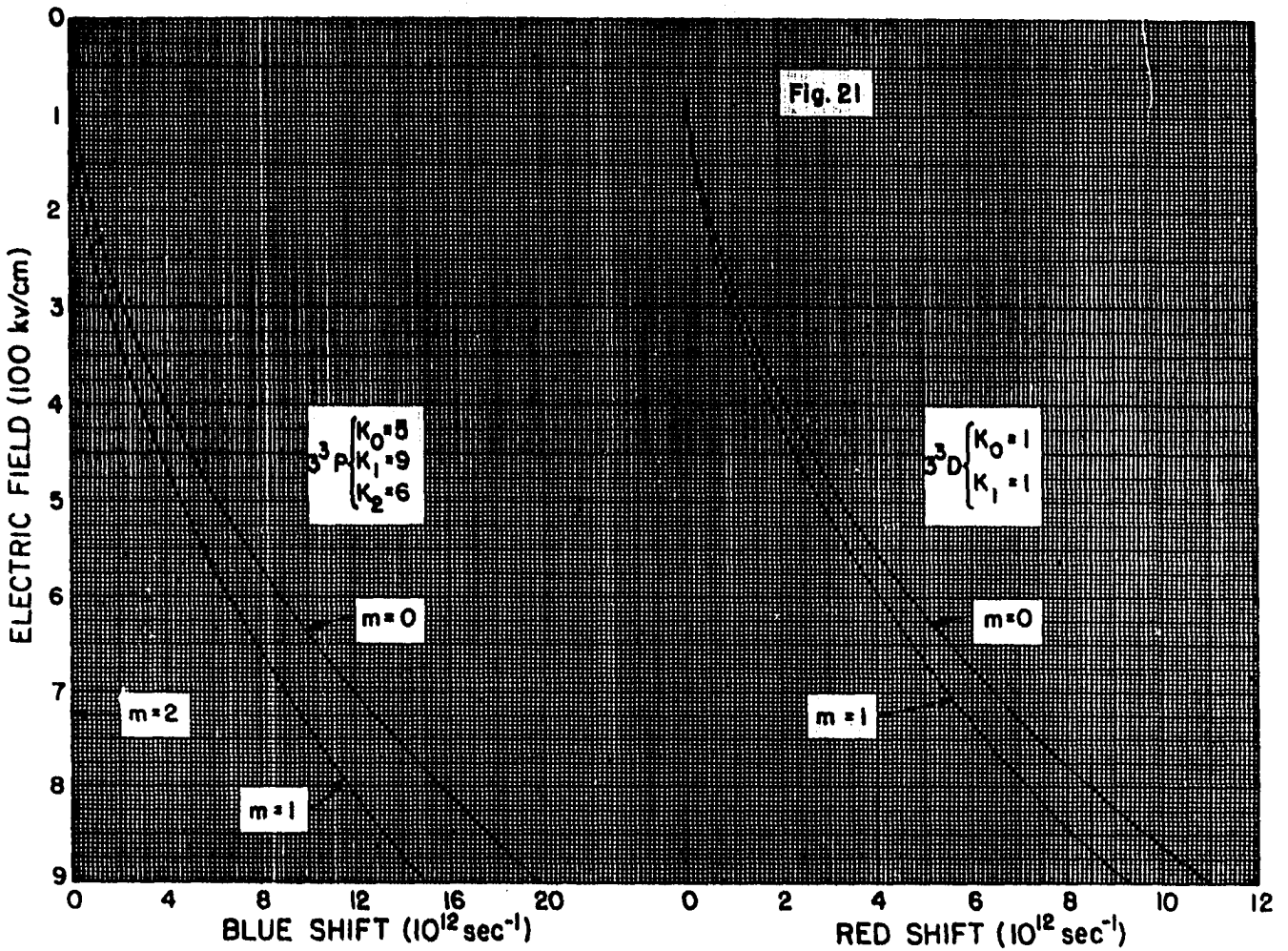

Fig. 21. Static Stark Effect, Second Order

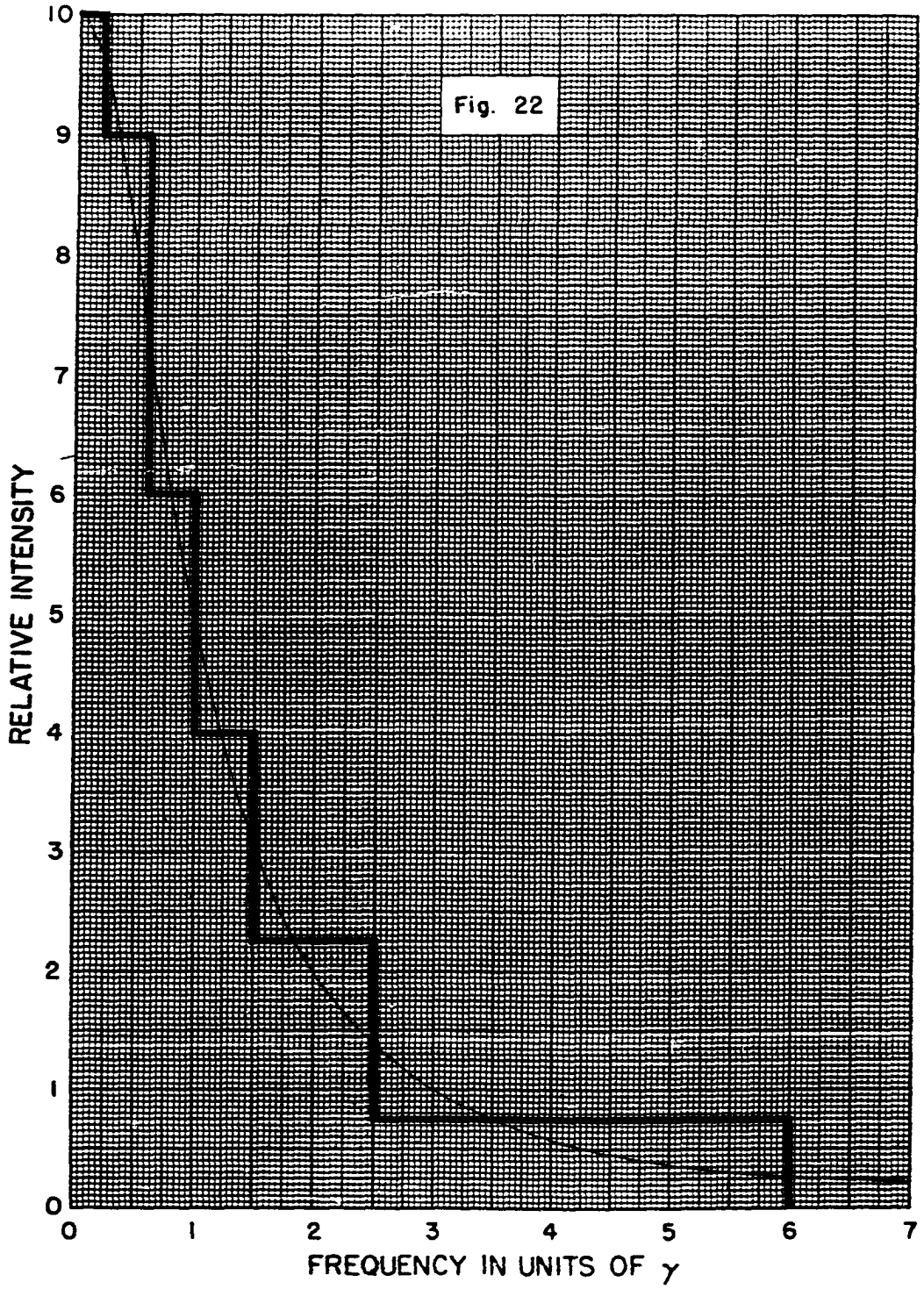

Fig. 22. Step Approximation to a Dispersion Line Shape

(VI-4). The area or strength, K_m, for each component is proportional to the sum of the intensities of the transitions originating in state n,ℓ,m. Values for K_m were obtained from Condon and Shortley.[8]

Consider only one component, say that for m, with an intensity $I[\nu, \nu_o(F)]$ where ν_o is the position of the center of the component and F is the field strength. If the probability that a field exists is $W(F)dF$, then the resultant profile of the Stark component will be

$$I(\nu) = \int_0^\infty I[\nu, \nu_o(F)]\ W(F)dF \qquad \text{(VI-5)}$$

where it is assumed that $I[\nu, \nu_o(F)]$ is represented by the stepped shape shown in Fig. 22.

$I(\nu)$ can be evaluated numerically if Eq. (VI-5) is rewritten, in terms of Fig. 22, as

$$I(\nu,m) \simeq K_m \left[0.75 \int_{F(\nu-6\gamma)}^{F(\nu+6\gamma)} W(F)dF + 1.5 \int_{F(\nu-2.5\gamma)}^{F(\nu+2.5\gamma)} W(F)dF + 1.75 \int_{F(\nu-1.5\gamma)}^{F(\nu+1.5\gamma)} W(F)dF \right.$$
$$\left. + 2 \int_{F(\nu-\gamma)}^{F(\nu+\gamma)} W(F)dF + 3 \int_{F(\nu-0.6\gamma)}^{F(\nu+0.6\gamma)} W(F)dF + 1 \int_{F(\nu-0.2\gamma)}^{F(\nu+0.2\gamma)} W(F)dF \right] \qquad \text{(VI-6)}$$

Here the electron half width, γ, must be given in frequency units instead of radians per second, as in Eq. (VI-4). Thus $\gamma = \gamma_{n,\ell}/2\pi$.

The total line shape is then obtained by adding all of the components graphically. The shifted position is obtained by shifting the total

---

[8] E. U. Condon and G. H. Shortley, The Theory of Atomic Spectra (Cambridge University Press, London, 1953) p. 411.

shape by an amount $\acute{o}_{n,l}/2\pi$ as given by Eq. (VI-3).

Line profiles and positions predicted in the manner just described are shown in Fig. 23 for the lines at 3889 and 5876 A for an initial pressure of 20 mm Hg. This comparison with experimental results shows that the line at 5876 A was much broader than the theory predicted. This discrepancy was believed to be due to self-absorption of this very strong line and is discussed in the next section. No clear explanation has been found for the disagreement between theory and experiment in the case of the line at 3889 A, since the experimental width is less than that predicted, and consideration of self-absorption would only increase the disagreement.

Here it is interesting to note that the neglect of the effect of the electrons would have resulted in half width predictions of less than 1 and 4 A for the lines at 3889 and 5876 A, respectively. These values are clearly too small by an order of magnitude and show the necessity of considering electron effects.

The lines at 4713 and 5015 A are subject to the same treatment as was used on 3889 and 5876 A, but the quality of the experimental data for the profiles of these lines would not permit a useful comparison between theory and experiment.

Shifts have been calculated for the lines at 4713 and 5015 A and are compared with experiment in Figs. 24 and 25. The electron shift was obtained by using Eq. (VI-3). The curves marked "ion" are values of the average of the "mean ion shifts" of the Stark components. This "mean ion shift" was obtained by using Holtsmark's most probable field, $F_{m.p.} = 3.26\, en_e^{2/3}$ in Eq. (VI-1). If the effects of the ions and electrons are

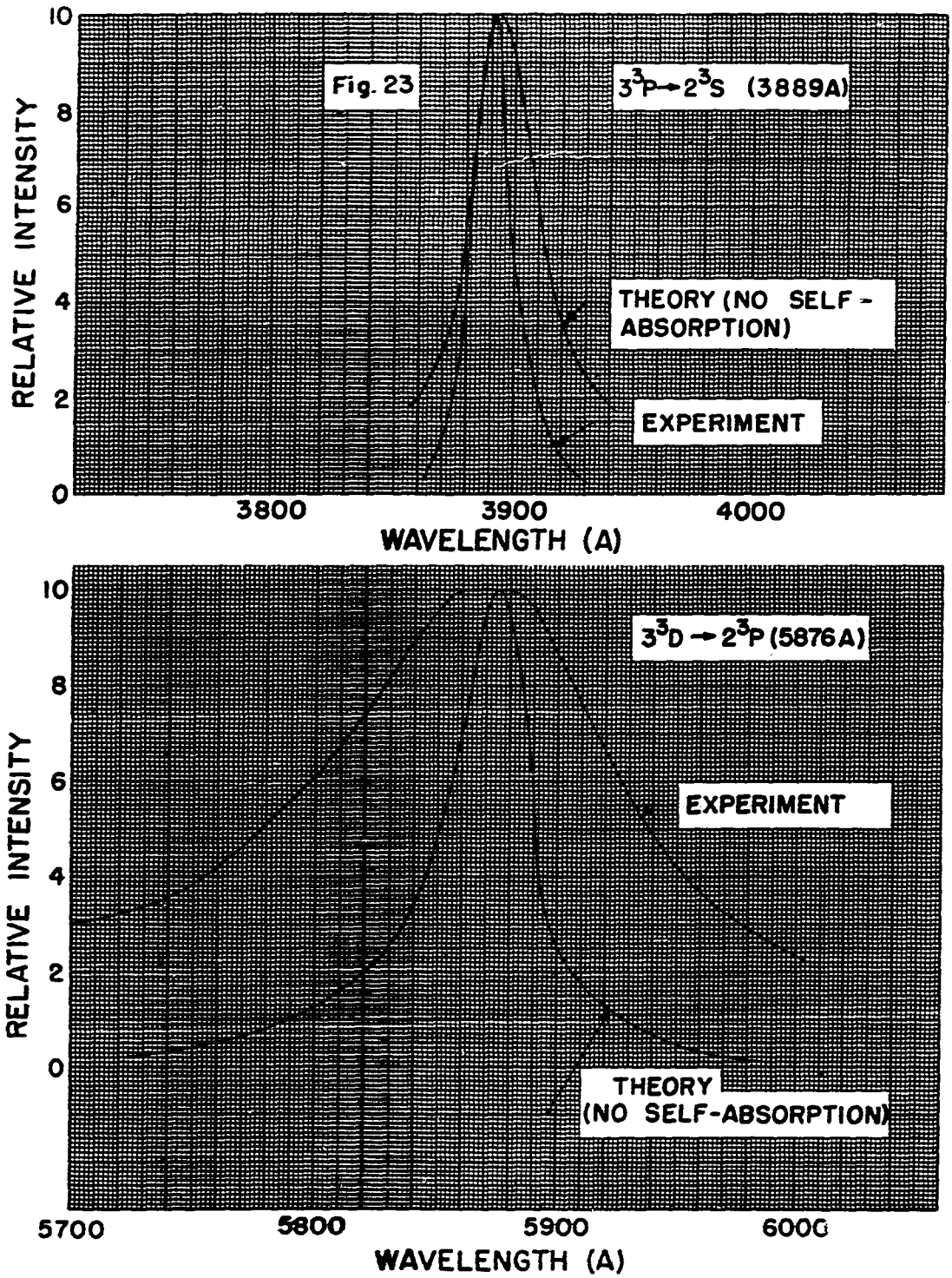

Fig. 23. Comparison of Theory (Neglecting Self-absorption) with Experiment

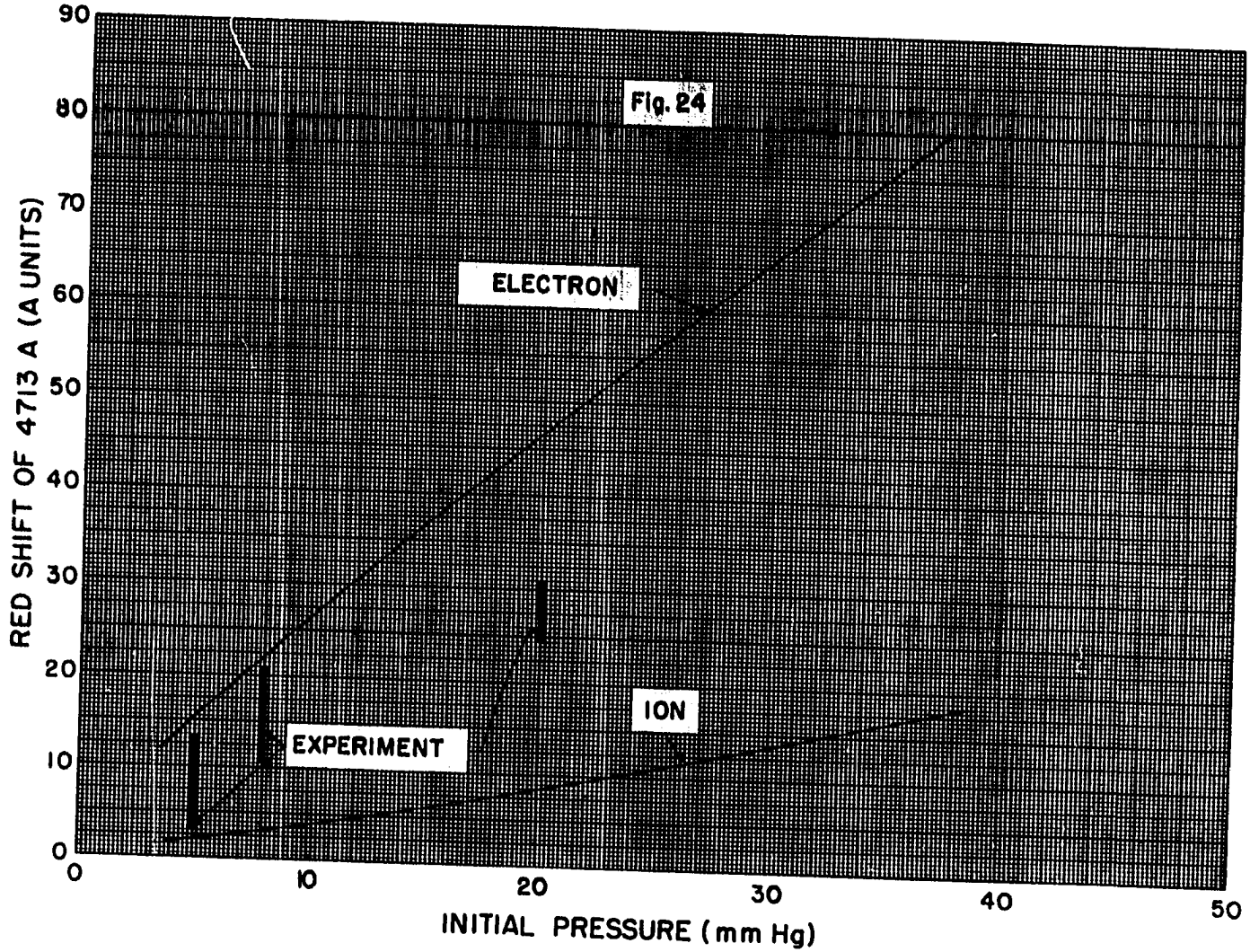

Fig. 24. Shift of the Line at 4713 A

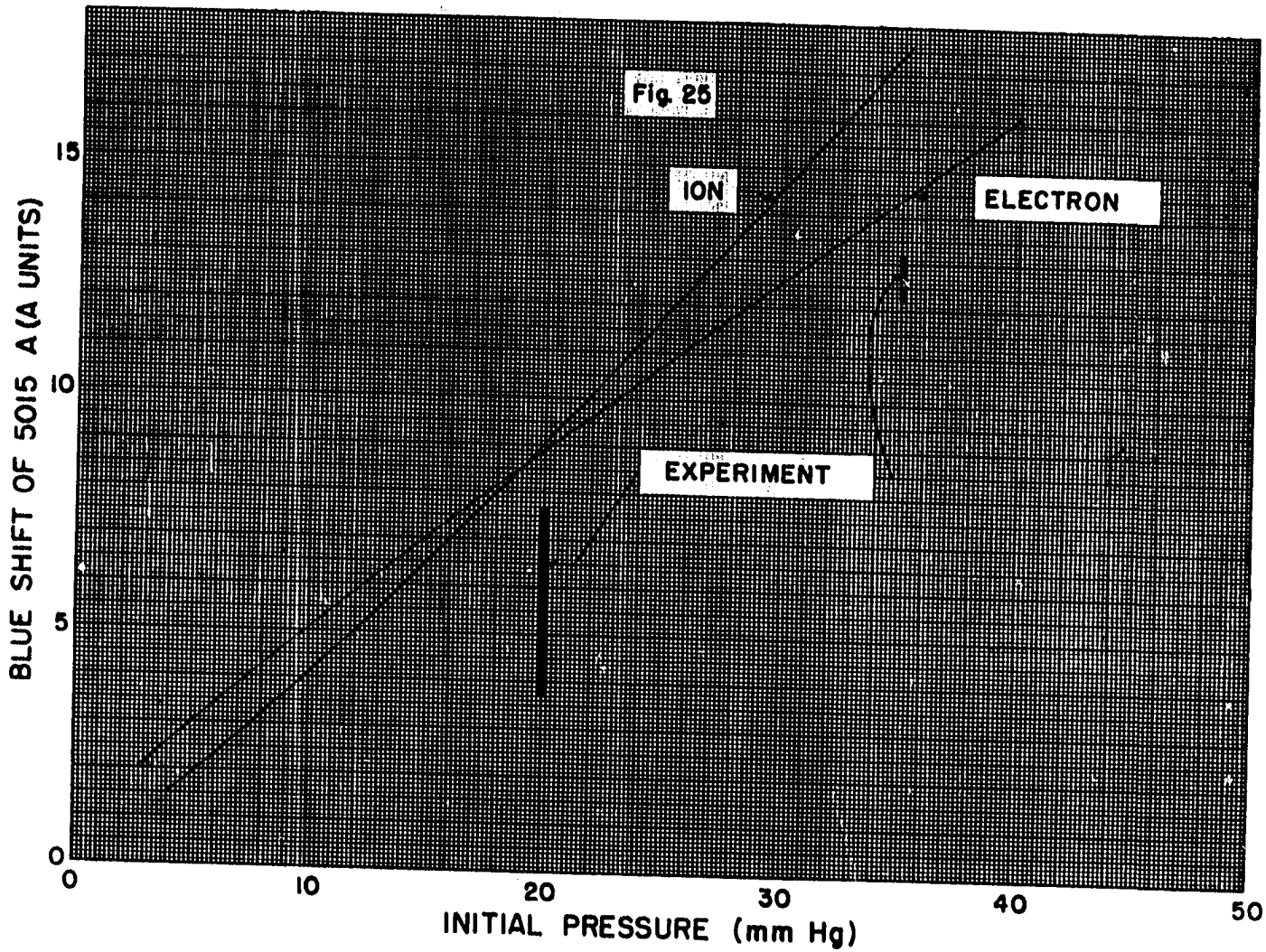

Fig. 25. Shift of the Line at 5015 A

added linearly then the theoretical predictions are always much larger than the measured values.

Self-absorption Broadening

When a spectral line is emitted by a gas sample having a finite thickness, the line will appear broader as the sample thickness is increased. Consider the simple case of a column of gas of unit cross section which emits collimated light uniformly in the positive x direction.

Let the rate of emission per unit length be $c\mu(\nu)$. At x let there be an intensity $I(\nu,x)$ erg/cm^2 sec in the direction of increasing x. On passing through dx, part of $I(\nu,x)$ is absorbed and the simplified transfer equation becomes

$$dI(\nu,x) = - I(\nu,x)\ \mu(\nu)dx + c\mu(\nu)dx \qquad \text{(VI-7)}$$

or

$$\frac{dI(\nu,x)}{c-I(\nu,x)} = \mu(\nu)dx$$

Integration yields

$$I(\nu,x)-c = e^{-\mu(\nu)x+K} \qquad \text{(VI-8)}$$

where K is an integration constant. As $x\rightarrow\infty$, $I(\nu,x)\rightarrow I_B(\nu,T)$, where $I_B(\nu,T)$ denotes the radiation from the surface of a blackbody at temperature T. When this condition is substituted into Eq. (VI-8)

$$I(\nu,x) = I_B(\nu,T)\left(1-e^{-\mu(\nu)x}\right) \qquad \text{(VI-9)}$$

Thus to predict $I(\nu,x)$, the observed line shape, it is necessary to know, not only the functional dependence of μ on ν but also the absolute value of $\mu(\nu)$. Since emission and absorption line profiles are proportional,

$$\mu(\nu) = A\ I(\nu) = A\sum_m I(\nu,m) \qquad \text{(VI-10)}$$

where the $I(\nu,m)$ are obtained by the method leading up to Eq. (VI-6). An approximate value for A may be obtained by the method followed earlier for calculating losses due to line radiation. There the energy emitted per cubic centimeter per second in a given line was taken as

$$E_L = N_{1s^2}\, g_n\, e^{-E_n/kT} A_{nn',h\nu'}\ \text{erg/cm}^3\ \text{sec} \qquad \text{(VI-11)}$$

where the notation is defined on page 63. But $E_L = \int E(\nu)d\nu$, where $E(\nu)$ is the energy radiated per cubic centimeter per second per unit frequency, and the integral is taken over the line L. According to some relations given by Aller[9]

$$A_{nn',h\nu'} = \frac{4\pi}{h\nu}\,\frac{g_{n'}}{g_n}\,\frac{2h\nu'^3}{c^2}\int a(\nu)d\nu \qquad \text{(VI-12)}$$

where $a(\nu)$ is the atomic absorption coefficient and ν' is the position of the center of the line corresponding to the transition $n \rightarrow n'$. When Eq. (VI-12) is substituted into Eq. (VI-11)

$$E_L = \frac{8\pi h\nu'^3}{c^2} N_n\, g_{n'} \int a(\nu)d\nu = k\int I(\nu)d\nu \qquad \text{(VI-13)}$$

where k can be evaluated from a calculated value of E_L and a numerical integration over $I(\nu')$. Then

$$\int a(\nu)d\nu = \frac{kc^2}{8\pi h\nu'^3 N_n\, g_{n'}}\, I(\nu)d\nu = \frac{\mu(\nu)}{N}\, d\nu \qquad \text{(VI-14)}$$

When the integral signs are removed

$$\mu(\nu) = \frac{kNc^2}{8\pi h\nu'^3 N_n g_{n'}}\, I(\nu) = A\, I(\nu) \qquad \text{(VI-15)}$$

---

[9] L. H. Aller, Astrophysics (The Roland Press Company, New York, 1953).

The constant k, and therefore A, in Eq. (VI-15) depends on the arbitrary scale factor used in the calculation of $I(\nu)$ in the previous section. N is the particle density of neutral helium atoms. Equation (VI-9) for the observed line shape then becomes

$$I(\nu,x) = I_B(\nu,T)\left(1-e^{-AI(\nu)x}\right) \qquad \text{(VI-16)}$$

This approximate method for predicting absorption broadening has been applied to the lines at 3889 and 5876 A as calculated in the previous section. Resulting self-absorbed line profiles are shown in Fig. 26, where they are compared with the calculated profiles without self-absorption. A comparison with experimental results shows that, when self-absorption is considered, both lines are found to be narrower than the theory predicts.

Depression of the Series Limits

No spectral lines were observed which originated at energy levels with principal quantum numbers greater than 4. Inglis and Teller[10] have treated the depression of the series limits in one-electron spectra by determining the ion density necessary to cause broadened levels with different principal quantum numbers to overlap into a continuum. In a similar way, Eq. (VI-1) can be used to give an approximate value for the ion density necessary to cause merging of helium levels with different principal quantum numbers.

The He I lines at 4471 A (4^3D--2^3P) and 4713 A (4^3S--2^3P) were observed experimentally, although they were very broad, whereas the

---

[10] D. R. Inglis and E. Teller, Astrophys. J. 90, 439 (1939).

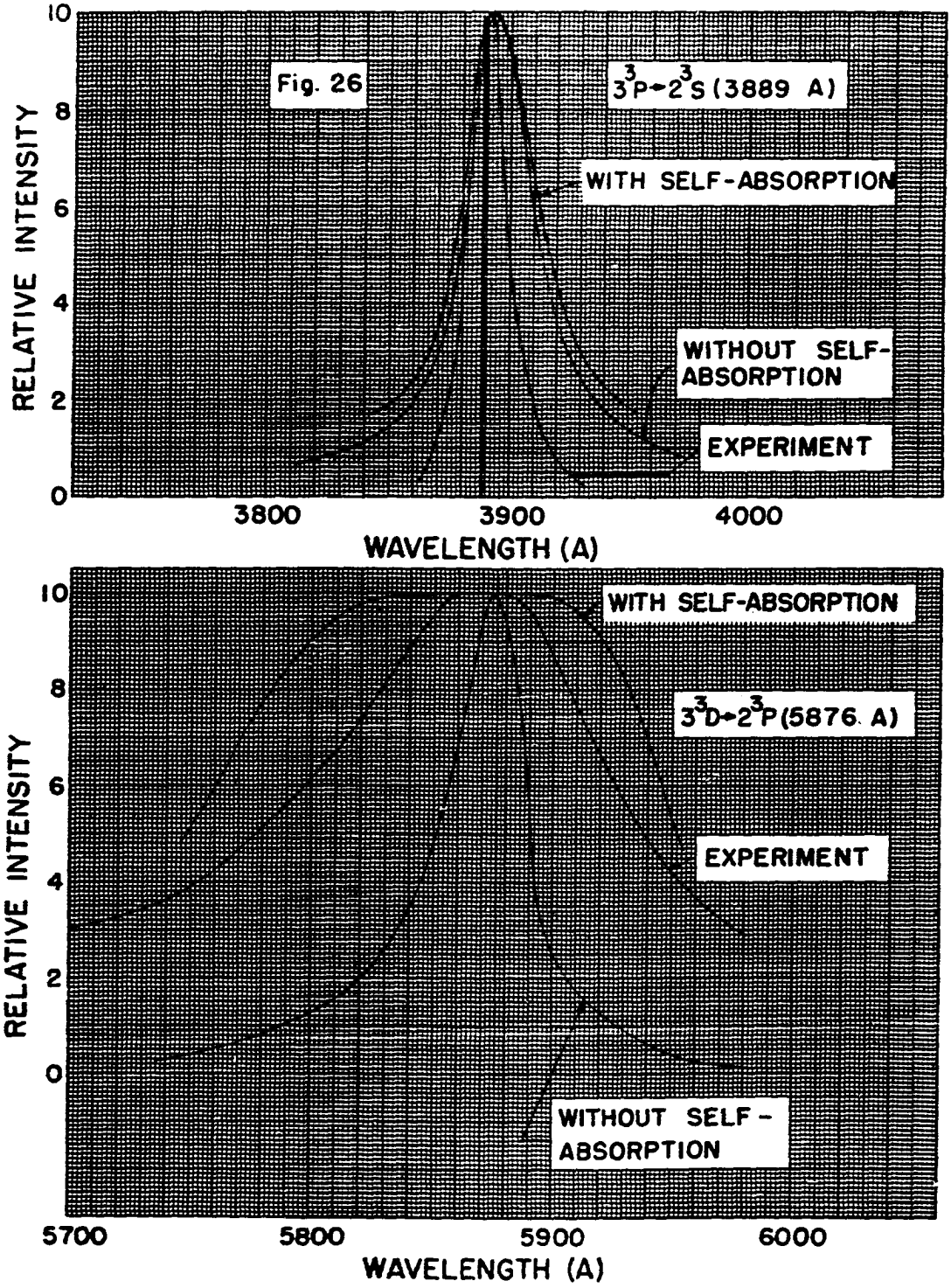

Fig. 26. Effect of Self-absorption on Theoretically Predicted Line Shapes

normally strong line at 4026 A (5^3D--2^3P) was never observed. This implies that the energy levels with principal quantum numbers 5 and greater are smeared together. A rough calculation based on Eq. (VI-1) indicates that the minimum ion densities obtained in the experiments, about 2×10^{17} cm^{-3}, would indeed permit observation of lines originating at levels with n = 4, but not those originating at levels with higher principal quantum numbers. If Holtsmark's estimate of the most probable field, $F_{m.p.} = 3.26\, e n_e^{2/3}$ is used, the shifts of the m = 0 Stark components of the levels 4^3D, 5^3D, and 6^3D are -359, -2350, and -3500 cm^{-1}, respectively. The effect of this "average width" is shown in Fig. 27. Stark components with m>0 are shifted by smaller amounts than those with m = 0 and electron broadening of 5^3D and 6^3D is small compared to the ion effect.

Thus an approximate theory would predict the series limits to be somewhere between levels with n = 4 and n = 5, and this is in agreement with observations.

Forbidden Lines

Lines were observed experimentally which corresponded to the normally forbidden transitions 3^3P--2^3P and 4^3F--2^3P. The appearance and intensities of these forbidden transitions can be predicted as a function of the electric field at the emitting atom.

These two forbidden lines will be treated separately. The line originating at the 3^3P level is subject to a treatment in which it is assumed that all ionic effects are proportional to the square of the electric field.[11] This assumption is valid as long as the perturbation of the

---

[11] H. Bethe, Handbuch der Physik (2d ed., Vol. 24, Part I; Verlag Julius Springer, Berlin, 1933).

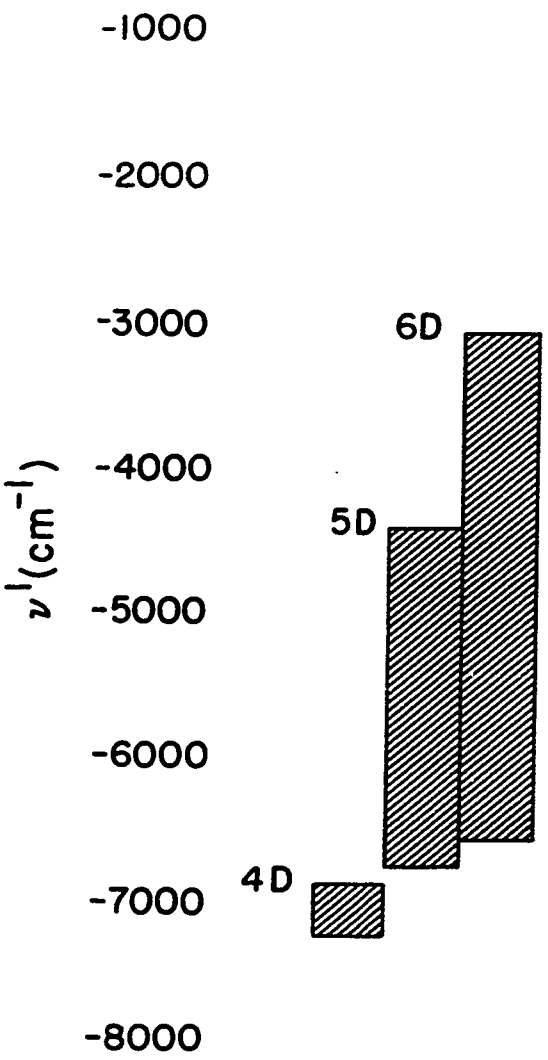

Fig. 27. Depression of Series Limits

energy level is small compared to the initial separation of the level from others with the same principal quantum number. If hydrogen wave functions and helium energy levels are used, a Schrodinger perturbation treatment gives, for the ratio of the intensity of the forbidden line to the intensity of the allowed line,

$$\frac{I_{n,l,m--n_o,l}}{I_{n,l+1,m--n_o,l}} = \frac{9}{4} \frac{F^2}{(E_{n,l+1}-E_{n,l})^2} \frac{[n^2-(l+1)^2]n^2[(l+1)^2-m^2]}{4(l+1)^2-1} \qquad \text{(VI-17)}$$

where F and E are expressed in atomic units. For the forbidden transition 3^3P--2^3P, which appears in the red wing of 5876 A in Fig. 11, this becomes, with F expressed in kv/cm

$$\frac{I_{3,P,0--2,P}}{I_{3,D--2,P}} = \frac{27\,F^2}{(E_{3,D}-E_{3,P})^2} = 0.167 \times 10^{-6}\,F^2$$

If Holtsmark's expression for the most probable field is again applied, a typical field found in the experiments is about 450 kv/cm. The above intensity ratio is then about 0.03. This value agrees to within an order of magnitude with experimental results. A precise measurement of the intensity ratio is difficult because the allowed and forbidden lines overlap, and the profile of neither is known.

Theoretically predicted values for the line shift of the 3^3P--2^3P transition are compared with experimental values in Fig. 28. The predicted shifts were obtained in the same way as were those plotted in Figs. 24 and 25.

The simplified theory for the intensity ratio used above is not valid for studying the forbidden transition 4^3F--2^3P because the pertur-

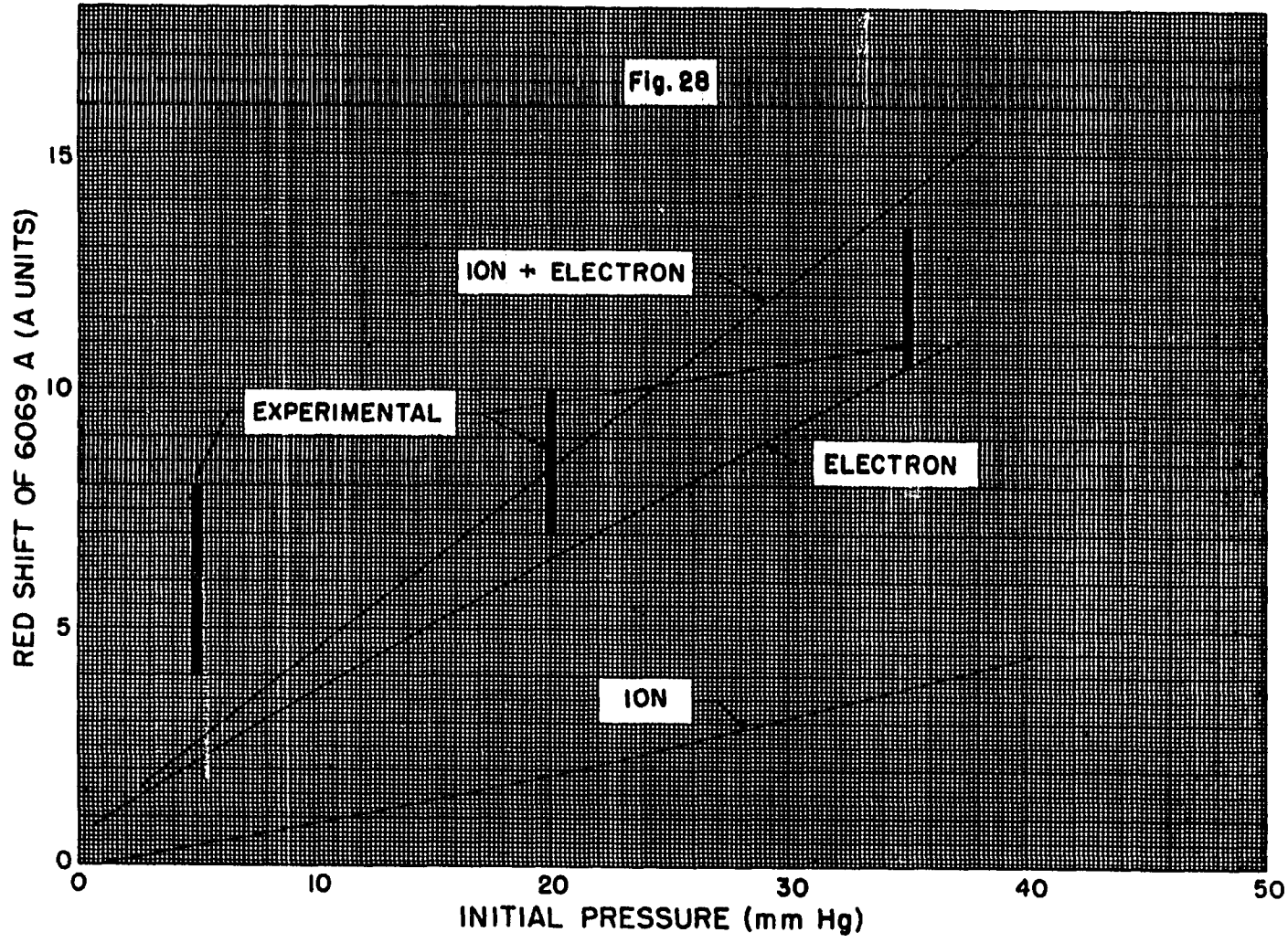

Fig. 28. Shift of the Line at 6069 A

bations of the levels 4^3D and 4^3F are greater than the initial energy separation. In his study of the Stark effect in helium, Foster[12] has treated the allowed and forbidden transitions, 4^3D--2^3P and 4^3F--2^3P in detail. He has tabulated line positions and intensities for fields ranging from 0 to 100 kv/cm. If these results are extended to include fields as strong as 450 kv/cm it is found that the intensity of the forbidden line should actually be slightly greater than that of the allowed line. Indeed, a rough analysis of the experimental results showed the forbidden line to be slightly the stronger in all cases.

Values for the shifts of the allowed-forbidden pair 4^3D--2^3P and 4^3F--2^3P were calculated as follows. The electron shift was obtained, as above, directly from Eq. (VI-3). To calculate the ion shift it was necessary to extend Foster's treatment of Stark splitting in helium up to stronger fields which corresponded to the ion densities found in the experiments. The ion shift was taken to be that of the strongest Stark component in the "most probable field," $3.26\ e n_e^{2/3}$. These values are plotted and compared with experimental results in Fig. 29. Figure 29 indicates that Foster's more thorough method of treating the helium Stark effect provides agreement with experiment. It is also interesting to note that the effect of the electrons is to shift both lines in the same direction and further improve the agreement with experiment.

Continuum Radiation

In some cases which were observed experimentally, continuum radiation formed a background for the broadened and shifted lines. The vari-

---

[12] J. S. Foster, Proc. Roy Soc. (London) A117, 137 (1927).

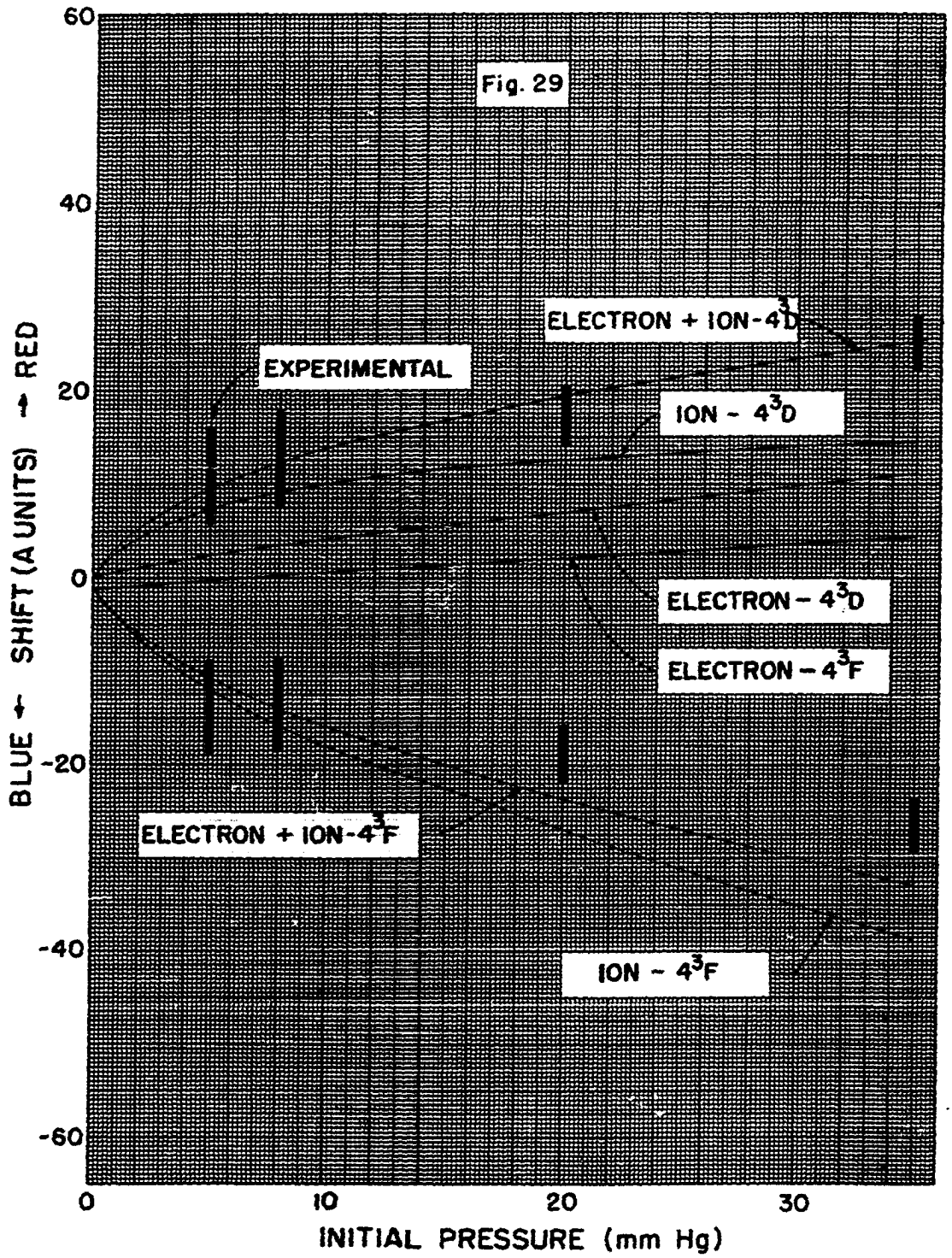

Fig. 29. Shift of the Allowed-Forbidden Pair at 4470 and 4471 A

ation of the ratio of the intensities of line spectra and continuum with thermodynamic state can be predicted and the results compared with experiment.

According to Eq. (VI-11), the total energy emitted in a line per cubic centimeter per second is approximately

$$E_L = N_{1s^2}\, g_n e^{-E_n/kT} A_{nn'} h\nu$$

Thus for a given line and for a given temperature, $E_L \propto N_{1s^2} \simeq N\text{-}n_e$ where N is the total number of helium nuclei per cubic centimeter.

Relations for the energy emitted in the form of continuum are found in Chapter 5. For bremsstrahlung

$$E_b \propto T^{1/2} n_e^2$$

and for recombination radiation

$$E_r \propto n_e^2$$

The temperature varied only slightly in the experiments, but the ion density, n_e, varied significantly with the intiial helium pressure in the shock tube, so

$$\frac{E_L}{E_b + E_r} \propto \frac{N\text{-}n_e}{n_e^2}$$

where E_L is the integrated energy in a line and $E_b + E_r$ is the continuum energy for any narrow region of the spectrum.

Evaluating $N\text{-}n_e/n_e^2$ for initial pressures of 20 and 35 mm Hg gives

$$R = \frac{\left(\frac{N-n_e}{n_e^2}\right)_{35 \text{ mm Hg}}}{\left(\frac{N-n_e}{n_e^2}\right)_{20 \text{ mm Hg}}} = 0.63 \pm 0.21$$

where the figure 0.21 is obtained by propagating the 90% confidence levels for the N's and n_e's through the calculation.

The experimental results presented in Table III which corresponded to R are 0.76 for the line at 3889 A and 0.71 for the line at 5876 A. At first glance these numbers might be interpreted as evidence that the line at 3889 A was self-absorbed at the higher pressure. No such conclusion can be drawn, however, since a deviation of about 2% in the shock velocity would cause a change of about 25% in the value of R.

CHAPTER VII

SUMMARY, CRITIQUE, AND SUGGESTIONS FOR FUTURE EXPERIMENTS

The data obtained from the experiments and hydrothermodynamic calculations provide a direct answer to the question: What is the appearance of the visible emission spectrum of helium when the temperature is about 20,000°K and the ion and electron densities are about 10^{18} cm^{-3}? Clearly, all observable lines were broadened and shifted; only a few lines were observable; one line was significantly self-absorbed; forbidden transitions appeared; and an appreciable quantity of continuum radiation was present. The extent of the broadening and shift of the spectral lines showed emphatically that the predicted effect of ion fields was not sufficient to explain the observations. Inclusion of the effect of the free electrons in perturbing the emitting atoms provided more satisfactory agreement between theory and experiment.

An additional consideration was necessary to explain the observed profile of the strong He I line at 5876 A. It was necessary to consider the effect of self-absorption broadening for this line in order to attain reasonable predicted line shapes.

The depression of series limits was found to be in agreement with predictions based on a simplified theory of line broadening by ion fields.

Two forbidden transitions, 3^3P--2^3P and 4^3F--2^3P were observed to

have positions and intensities which were approximately in agreement with theoretical predictions. The 4^3F--2^3P line is of particular interest since it was found that the separation of the forbidden-allowed pair, 4^3F--2^3P and 4^3D--2^3P could be predicted theoretically to within a small fraction of the total separation. Thus the splitting of this pair of lines could be used as a measure of the ion and electron density in a gas where conditions are unknown.

Continuum radiation was not studied in any detail, but it was found that, within the experimental precision, the ratio of the total energy emitted in a line to the energy emitted in a narrow band of continuum was proportional to $N\text{-}n_e/n_e^2$, where N and n_e are the densities of helium nuclei and helium ions, respectively.

Rough measurements of electronic excitation and ionization relaxation time at the shock front indicated an increase with decreasing gas density, as expected.

Certain useful techniques were developed during the course of the work. The conventional shock tube was modified by replacing the driver section with a block of high explosive from which emerged a plane shock wave. This system has as advantages greater potential shock strengths and the initial production of a plane wave in the shocked gas. On the other hand, these advantages are opposed by the complete destruction of the shock tube when it is fired. Much work remains to be done in the development of the explosive shock tube to a state where it can bridge the gap in shock strengths between those obtainable in the conventional shock tube and those discussed in this thesis.

The method used for making time-resolved spectra in these experi-

ments required no modifications to the spectrograph, thus allowing the use of any instrument merely by setting it in place with respect to the external optical system. The system which was used had an effective aperture of about f/16 and provided better than 1 μsec time resolution. A new set of components is presently on order which, when used in the same manner, should have an effective aperture of about f/3. This system then should resolve better than 0.1 μsec on a spectrogram.

One essential feature of the time-resolving spectrograph is a synchronizer which will fire the explosive charge at a predetermined position of the rotating mirror. A synchronizer with a reproducibility of better than 0.1 μsec is presently being developed for use with the new spectrograph.

The proposed system for time-resolving spectra will have the following characteristics:

effective aperture	f/3
response time	0.1 μsec (minimum)
total recorded time	2 μsec (with minimum response time)
dispersion	20 A/mm

Such a system will find many applications in the study of rapidly changing phenomena in which either emission or absorption spectra can be observed.

The usefulness of data from more refined experiments of the sort already performed could be improved by an absolute measurement of the light emitted by the shocked gas as a function of wavelength. Although experimentally a difficult problem, such a measurement would check calculations of radiative energy losses, and provide f-numbers for the ob-

servable helium lines.

One of the primary limiting features in the experiments was the large photographic grain size on the spectrograms. The additional light-gathering power of the proposed f/3 spectrograph will permit use of spectrograph plates with less granularity, and thus give better data on line profiles and positions.

This research has aroused interest in some additional problems. The nonequilibrium relaxation processes taking place at the front of a strong shock wave in helium might be studied in some detail by time-resolved spectroscopy. Measurements of time rates of change of line shapes, positions, and intensities combined with measurement of the rate of change of continuum intensity and distribution would provide part of a time-dependent partition function which might be related to the kinetic processes in the shock front.

Further study of the forbidden transition 4^3F--2^3P is indicated. Investigations of this line with decreasing ion densities might provide a check on the effects of a nonhomogeneous field predicted by Mrs. Krogdahl.[1]

It has been suggested that line absorption coefficients and thus line profiles might be investigated more thoroughly by merely placing a plane mirror behind the shock tube so that the spectrograph would see not only the light emitted toward it but also that which is emitted in the opposite direction and is reflected from the mirror. A comparison of spectra taken with and without the mirror would reveal the extent of self-absorption over a line profile.

---

[1] M. K. Krogdahl, Astrophys. J. 100, 333 (1944); 102, 64 (1945).